Cell Reports

Article

Hypothalamic astrocytic-BMAL1 regulates energy homeostasis in a sex-dependent manner

Graphical abstract

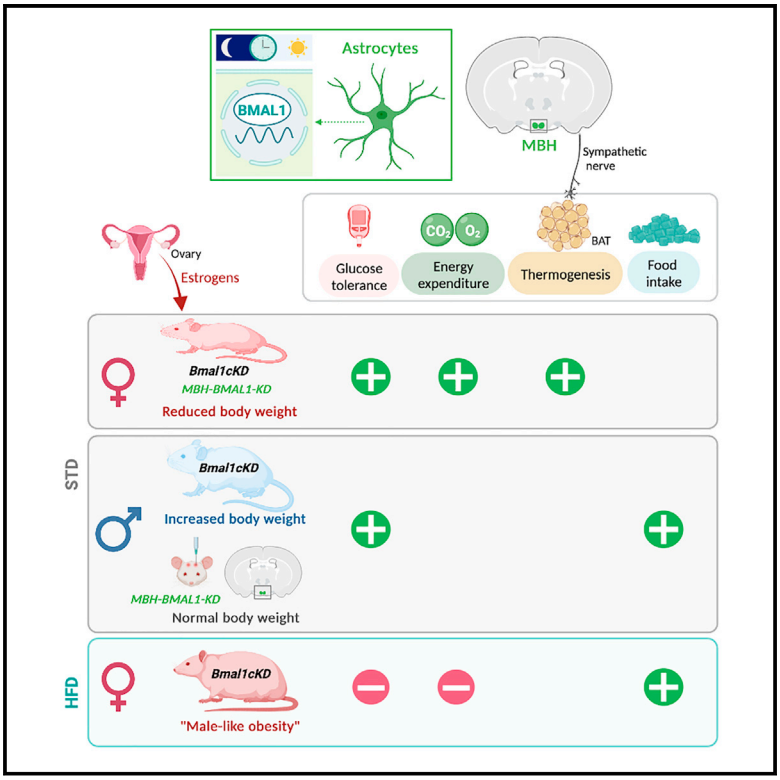

Highlights

- Astrocytic BMAL1 has a sexually dimorphic effect on energy homeostasis and obesity
- BMAL1 KD in hypothalamic female astrocytes leads to a negative energy balance
- BMAL1 KD in female mice yields male-like metabolic traits on high-fat diet

Authors

María Luengo-Mateos, Antía González-Vila, Nathalia Romanelli Vicente Dragano, ..., Paula Novelle-Rodríguez, Miguel López, Olga Barca-Mayo

Correspondence

m.lopez@usc.es (M.L.), olga.barca.mayo@usc.es (O.B.-M.)

In brief

Luengo-Mateos et al. uncover the sex-specific impact of hypothalamic astrocytic BMAL1 on energy balance. Surprisingly, knockdown of BMAL1 in female astrocytes results in negative energy balance while, intriguingly, leading to male-like metabolic obesity upon high-fat diet consumption. These findings underscore the crucial role of BMAL1 in regulating energy homeostasis.

Luengo-Mateos et al., 2023, Cell Reports *42*, 112949
August 29, 2023
https://doi.org/10.1016/j.celrep.2023.112949

CellPress

Cell Reports

CellPress
OPEN ACCESS

Article

Hypothalamic astrocytic-BMAL1 regulates energy homeostasis in a sex-dependent manner

María Luengo-Mateos,[1] Antía González-Vila,[1] Nathalia Romanelli Vicente Dragano,[1,2] Nataliia Ohinska,[1,3] María Silveira-Loureiro,[1] Marco González-Domínguez,[1] Ánxela Estévez-Salguero,[1] Paula Novelle-Rodríguez,[1] Miguel López,[1,2,*] and Olga Barca-Mayo[1,4,*]

[1]Physiology Department, Molecular Medicine, and Chronic Diseases Research Centre (CiMUS), University of Santiago de Compostela, 15782 Santiago de Compostela, Spain

[2]CIBER Fisiopatología de la Obesidad y Nutrición (CIBERobn), 15706 Santiago de Compostela, Spain

[3]Horbachevsky Ternopil National Medical University, 46001 Ternopil, Ukraine

[4]Lead contact

*Correspondence: m.lopez@usc.es (M.L.), olga.barca.mayo@usc.es (O.B.-M.)

https://doi.org/10.1016/j.celrep.2023.112949

SUMMARY

Here, we demonstrate that hypothalamic astrocytic BMAL1 computes cyclic metabolic information to optimize energetic resources in a sexually dimorphic manner. Knockdown of BMAL1 in female astrocytes leads to negative energy balance and alters basal metabolic cycles without affecting circadian locomotor activity. Thus, astrocytic BMAL1 contributes to the control of energy balance through the modulation of the metabolic rate, hepatic and white adipose tissue lipogenesis, and the activity of brown adipose tissue. Importantly, most of these alterations are specific to hypothalamic astrocytic BMAL1. Moreover, female mice with BMAL1 knockdown in astrocytes exhibited a "male-like" metabolic obese phenotype when fed a high-fat diet. Overall, our results suggest a sexually dimorphic effect of astrocytic BMAL1 on the regulation of energy homeostasis, which may be of interest in the physiopathology of obesity and related comorbidities.

INTRODUCTION

Homeostasis in mammals is maintained by complex mechanisms that regulate the balance between energy intake and expenditure.[1,2] Circadian rhythms, primarily controlled by the hypothalamic suprachiasmatic nucleus (SCN), play a crucial role in maintaining homeostatic regulation.[3,4] Neurons and astrocytes within the SCN coordinate circadian physiology and behavior generated by cell-autonomous oscillators present in nearly every cell of the body.[5–11] Light entrains the SCN, which conveys temporal information to other brain and peripheral clocks through neuronal, hormonal, or behavioral activity rhythms, such as the feeding-fasting and sleep-wake cycles.[12,13]

The molecular clock, a molecular machinery present in virtually every cell and tissue, governs the intimate interplay between nutrition, metabolism, exercise, and circadian physiology.[14] Composed of transcriptional-translational feedback loops, the molecular clock involves E-box specific transcription factors BMAL1 and CLOCK, which activate the transcription of clock-controlled genes influencing energy homeostasis.[15] Disruption of the circadian cycle is strongly linked to metabolic imbalance, as observed in individuals working night shifts or experiencing circadian arrhythmia in rodent models.[3,16–18] The circadian function of BMAL1 is tightly linked to the principal metabolic processes of cells and tissues. For instance, BMAL1 ablation in white adipose tissue (WAT) leads to obesity and altered feeding rhythms, while its absence in brown adipose tissue (BAT) impairs thermogenesis.[19,20] In astrocytes, BMAL1 controls molecular, physiological, and behavioral circadian rhythms, affecting cognition, locomotor activity, glucose metabolism, and insulin sensitivity in male mice.[4,7,8,10,11,17]

Sex differences have been observed in circadian rhythms, with females exhibiting shorter periods and higher-amplitude oscillations in gene expression.[21,22] Estrogens are not necessary for maintaining circadian rhythms, while testosterone limits the phase-shifting effect of light.[23,24] Females also demonstrate greater resistance to genetic and environmental circadian disruption compared with males.[25] Interestingly, circadian processes such as metabolism, feeding, sleep-wake cycles, hormone secretion, cardiovascular function, and body temperature regulation display sex dimorphism, but the underlying regulatory circuits and signaling mechanisms remain poorly understood.

This study aimed to investigate the impact of sex on the actions of astrocytes in energy balance by affecting the metabolic rate, lipogenic enzymes in the liver and WAT, and BAT thermogenesis. Importantly, these effects are influenced by both sex and diet. Notably, mice with BMAL1 knockdown in female astrocytes exhibited a male-like metabolic obese phenotype when fed a high-fat diet. These results provide valuable insights into the role of astrocytes in regulating energy balance and their dependence on sex.

RESULTS

Impact of female astrocytic BMAL1 in circadian locomotor behavior

We examined the impact of astrocytic BMAL1 on circadian locomotor behavior in female mice using a tamoxifen (TM)-inducible knockdown mouse model (*Bmal1*$^{flx/flx}$, *Glast-CreERT2*$^{+/-}$, referred to as Bmal1cKD [conditional knockdown]).[11,17,26] Previous studies have characterized the efficiency and specificity of BMAL1 KD in the SCN and other hypothalamic nuclei in males.[11,17] To evaluate the recombination efficiency in female mutants, we crossed Bmal1cKD mice with a Cre-inducible red fluorescent reporter mouse line (Td-Tomato). TM was administered to Bmal1cKD-Td-Tomato females and controls (*Glast-Cre*-Td-Tomato) following a validated approach used in males.[11,17,26,27] Co-localization analysis confirmed a significant 50% reduction in BMAL1-positive astrocytes in the SCN (Figures S1A and S1D) and the hypothalamic arcuate nucleus (ARC) (Figures S1E and S1H) of *Bmal1cKD*-Td-Tomato females compared with controls, consistent with findings in male *Bmal1cKD*s.[11,17] Furthermore, a decrease in BMAL1-positive cells among Td-TOMATO- or GFAP-negative cells was observed in the SCN (Figures S1B–S1D) and the ARC (Figures S1F–S1H) of *Bmal1cKD* females, suggesting an impact of female astrocytes on the neuronal clock, similar to studies in males.[9–11,17,28]

We monitored circadian locomotor activity in female mice following entrainment to a 12-12 h light-dark (LD) cycle, transfer to constant darkness (DD), and subsequent re-entrainment to a new LD cycle (rLD).[11] Bmal1cKD females entrained to LD cycles and exhibited comparable periodicity to controls (23.90 ± 0.05 and 23.86 ± 0.03, paired t test p = 0.5470) (Figures S1I–S1K). Notably, mutant mice exhibited increased activity during the first half of the dark phase, suggesting a potential role for astrocytic BMAL1 KD in shaping activity profiles during the dark (Figure S1I). In DD, both control and Bmal1cKD females displayed a similar daily rhythm with an approximately 24 h period (24.02 ± 0.04 and 24.02 ± 0.03, paired t test p = 0.97) (Figures S1I–S1K), indicating that the mutants did not exhibit an increased period as observed in males.[7,8,10] Following the DD period, Bmal1cKD females adjusted their activity to a new LD cycle, similar to controls (Figures S1I–S1K), but still showed increased activity during the first half of the dark period (Figure S1I).

These findings suggest that the specific KD of astrocytic BMAL1 does not significantly influence circadian locomotor behavior in female mice. It is possible that the remaining BMAL1-positive SCN astrocytes are sufficient to maintain circadian locomotor behavior in females.

BMAL1 KD in astrocytes regulates energy balance in a sex-dimorphic fashion

We studied the metabolic phenotype of *Bmal1cKD* mice, comparing male and female controls (*Bmal1*$^{fl/fl}$) with *Bmal1cKD* littermates on a standard diet (STD) for 20 weeks.[17] Female *Bmal1cKD* mice had lower body weight than controls during weeks 3–14 after TM treatment (Figure 1A), despite increased feeding (Figure 1B) and similar activity levels (Figure 1C). They also had significantly reduced lean mass 8 weeks after TM treatment (Figure 1D). At 17 weeks after TM treatment, female mutants had had body weight and composition similar to controls, except for increased gonadal fat mass (Figure S2A). In contrast, as previously reported, male mutants exhibited higher body weight than controls after 17 weeks of TM treatment (Figure S2B),[17] along with normal levels of spontaneous activity[11] (Figure S2C). Moreover, male Bmal1cKDs displayed higher absolute adipose tissue mass than controls due to increased gonadal fat mass (Figure S2D). Female *Bmal1cKD*s displayed a blunted daily glucose level oscillation (Figure 1E), whereas males maintained glucose level oscillation with lower daily levels.[17] After fasting, no differences in glucose levels were observed in female mutants (Figure 1E). Glucose and insulin (INS) tolerance tests (GTTs and ITTs) showed that *Bmal1cKD* females had significantly improved glucose tolerance (Figure 1F) and normal INS sensitivity (Figure 1G), similar to males (Figure S2E).[17]

To investigate the involvement of ovarian function in the observed sex differences, we performed bilateral ovariectomy (OVX) or sham operations on control or *Bmal1cKD*s 4 weeks after TM treatment when mutants started showing decreased body weight (Figure 1H). Two weeks after the procedure, OVX controls and mutants showed similar weight gain (Figure 1H). Although OVX mice did not display hyperphagia 4 weeks post-procedure,[29] OVX *Bmal1cKD*s increased and normalized daytime food intake, as previously reported[30,31] (Figure 1I). Glucose tolerance in OVX mutants was comparable to controls (Figure 1J). Importantly, fat depots in control animals remained unaffected by OVX, as reported.[32] However, OVX mutants exhibited increased adiposity (Figure 1K) due to higher gonadal (g), subcutaneous (sc), and visceral (v) WAT depots (Figure 1L). Serum triglycerides, cholesterol, and liver triglycerides did not differ between controls and mutants at 9 weeks post-surgery (Figure 1M).[33–35] Interestingly, sham operated *Bmal1cKD*s exhibited lower triglycerides and a trend toward decreased serum cholesterol and liver triglycerides compared with sham controls (Figure 1M). These results indicate the crucial role of ovarian function in the metabolic phenotype of *Bmal1cKD*s, as bilateral OVX fully reversed the differences in body weight, glucose homeostasis, food intake, and serum lipid levels between controls and *Bmal1cKD*s.

While wheel running[11] and physical activity in the absence of a wheel showed a correlation in male *Bmal1cKD*s (Figure S2C), no such correspondence was observed in female mutants. Despite increased running-wheel activity (Figure S1I), female *Bmal1cKD*s exhibited comparable spontaneous activity to controls (Figure 1C). To further explore this, we analyzed the exploratory behavior and anxiety of male and female *Bmal1cKD*s in a novel environment using the open-field paradigm. Control and mutants showed habituation to the new environment within each session, as indicated by reduced distance traveled on day 2 compared with day 1 (Figure S2F). Similarly, the time spent in the center of the open field (Figure S2G) and the overall activity (Figure S2H) were unaffected by the genotype of the animals. Therefore, female *Bmal1cKD*s did not show anxiety, novelty-induced hyperactivity in locomotion, or deficits in habituation, consistent with previous findings.[36,37] However, the increased running activity of female mutants suggests a potential impact

CellPress
OPEN ACCESS

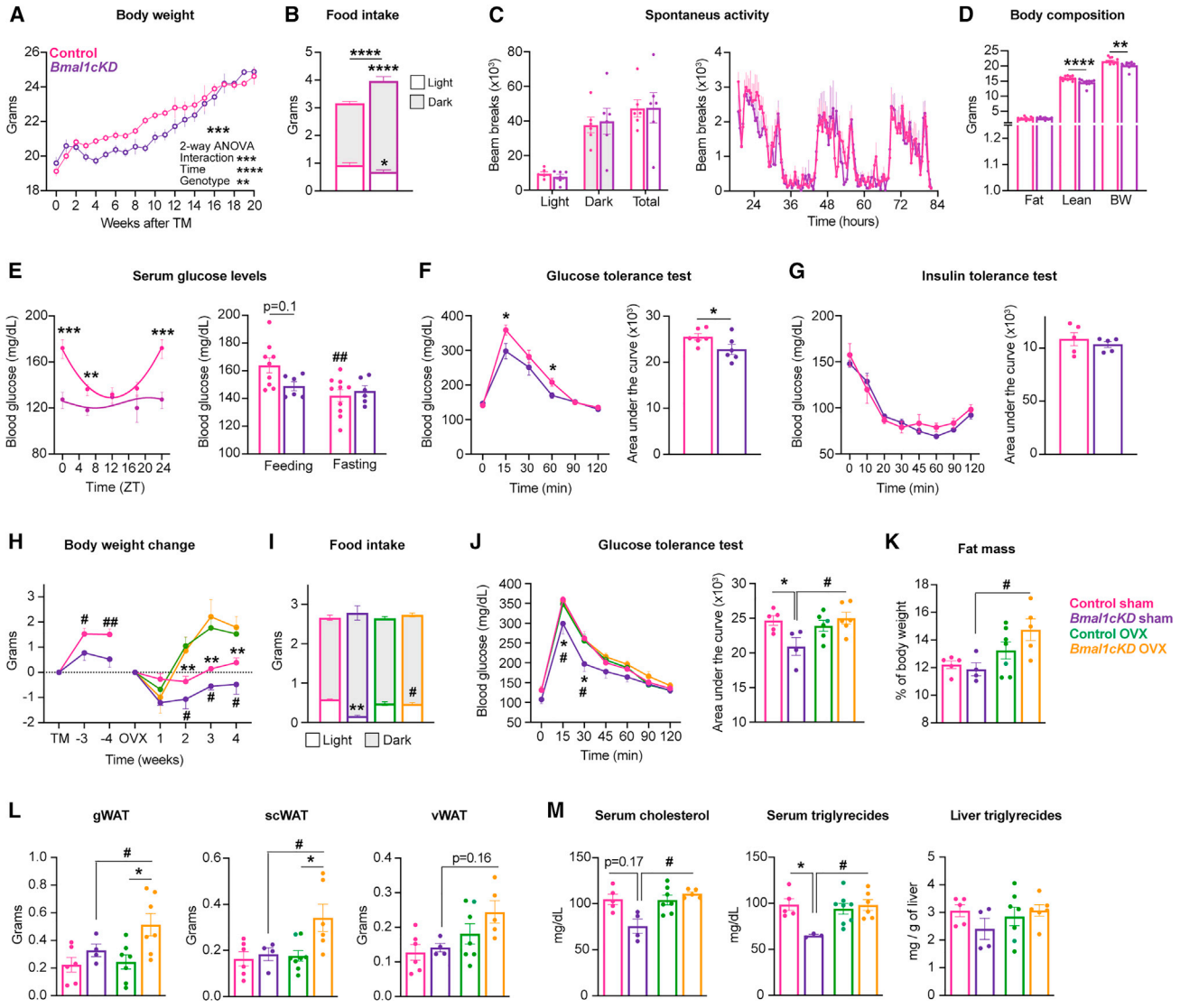

Figure 1. BMAL1 knockdown in astrocytes regulates energy balance in a sex-dimorphic fashion

(A) Age-dependent changes in body weight of control and *Bmal1cKD* females (n = 16).

(B) Food intake in control and Bmal1cKD females 8 weeks after of TM treatment (n = 8, paired t test, *p ≤ 0.05 and ****p ≤ 0.0001 vs. controls).

(C) Total spontaneous activity and daily activity waveforms for controls and *Bmal1cKD* mice after 8 weeks of TM treatment (n = 5–6).

(D) Fat and lean mass of control and *Bmal1cKD* females 8 weeks after of TM treatment (BW [body weight]) (n = 8, paired t test, **p ≤ 0.01).

(E) Serum glucose and fasting glucose levels in control and mutant females after 8 weeks of TM treatment. Experimental data were cosine fitted (n = 6–10, two-way ANOVA, ***p ≤ 0.001; ##p < 0.01 vs. fed animals).

(F and G) GTT (F) and ITT (G) in control and *Bmal1cKD* females 14–15 weeks after TM treatment at ZT10 (n = 5–6, paired t test).

(H) Age-dependent BW changes in sham and ovariectomy (OVX) control and mutants (n = 4–6, two-way ANOVA, #p < 0.05, ##p < 0.01 vs. controls; **p < 0.01 vs. OVX controls, and #p < 0.05 vs. OVX *Bmal1cKD*s).

(I) Daily food intake of control and OVX control and *Bmal1cKD* females 4 weeks after OVX or sham procedure (n = 4–6, two-way ANOVA, **p < 0.01 vs. sham controls; #p < 0.05 vs. sham *Bmal1cKD*s).

(J) GTT of control and OVX control and *Bmal1cKD* females 5 weeks after OVX or sham surgery performed at ZT10 (n = 4–6, two-way ANOVA).

(K) Fat mass of sham and OVX control and *Bmal1cKD* females 5 weeks after OVX or sham surgery (n = 4–7, two-way ANOVA).

(L) Weights of gonadal, subcutaneous, and visceral white adipose tissues (gWATs, scWATs, and vWATs) of OVX and sham control and *Bmal1cKD* females after 9 weeks of the procedure (n = 4–8, two-way ANOVA).

(M) Serum cholesterol, triglycerides, and liver triglycerides in control and *Bmal1cKD* females after 9 weeks of the OVX at ZT0 (n = 3–8, two-way ANOVA). Data are presented as mean ± SEM.

of astrocytic BMAL1 on neuronal circuits influencing physical activity in females.

Astrocytic BMAL1 controls BAT thermogenesis and hepatic and WAT lipogenesis in females

To understand the feeding-independent decrease in body weight in female mutants, we analyzed their BAT interscapular temperature. At 11 week after TM treatment, *Bmal1cKD* females showed higher BAT temperature compared with controls (Figure 2A), while no differences were observed in males (Figure S3A). Accordingly, uncoupling protein 1 (UCP1) expression in BAT of female mutants was increased at both Zeitgeber time 10 (ZT0) and ZT12 (Figures 2B and 2C), while the expression of BMAL1 remained unchanged (Figure 2C). This suggests that the elevated temperature observed in female mutants is not caused by disrupted circadian clock function within BAT. To investigate whether the increased thermogenesis in *Bmal1cKD* mice resulted from increased sympathetic nervous system (SNS) activity mediated by astrocytes,[38] control and *Bmal1cKD* females were treated with the β3 adrenergic receptor (β3-AR)-specific antagonist, SR59230A, 11 weeks post-TM treatment. β-Adrenergic antagonism reduced BAT thermogenesis activation and BAT UCP1 expression in *Bmal1cKD*s (Figure S3B). This was associated with similar body weight gain compared with controls (Figure S3B). Thus, astrocytic BMAL1 regulates SNS output and BAT thermogenesis in females, potentially contributing to the decreased body weight observed in the mutants.

Astrocytic BMAL1 affects fat mass in both males and females. Thus, cholesterol and triglycerides levels were analyzed in both groups at 18 and 11 weeks after TM. Male *Bmal1cKD*s showed higher serum cholesterol levels at ZT0 compared with controls (Figure S3A), while no differences were observed in females (Figure 2D). Serum triglycerides levels were higher at ZT0 compared with ZT12,[39] with no variations between sexes or genotypes (Figures 2D and S3A). However, female mutants showed lower liver triglycerides at ZT0 (Figure 2E) and reduced liver fat content (Figure 2F). This was accompanied by decreased expression of critical lipogenic enzymes such as acetyl-CoA carboxylase (ACC) and fatty acid synthase (FAS) and a trend toward decreased levels of the transcription factor sterol regulatory element-binding protein (SREBP1c) at ZT0 (Figure 2G). Additionally, mutants also exhibited increased levels of the lipolytic phosphorylated hormone-sensitive lipase (HSL) at ZT0 (Figure 2G). These results suggest that astrocytic BMAL1 promotes hepatic lipid storage in females. Interestingly, controls exhibited reduced expression of ACC and SREBP1c at ZT12, consistent with increased lipogenesis during the active period in mice.[40–42] However, *Bmal1cKD* females did not show this daily variation in hepatic lipogenic enzyme expression (Figure 2G). Notably, the altered expression pattern in mutants throughout the day was independent of the hepatic clock, as the daily oscillations of *Bmal1*, *Cry1*, *Per2*, *Nuclear receptor subfamily 1 group D member 1* (*Rev-Erbα*), *Albumin D element-binding protein* (*Dbp*), and *Cytochrome P450 Family 7 Subfamily A Member 1* (*Cyp7a1*) were comparable with controls (Figures 2H and 2I). This suggests that the changes in hepatic lipogenic enzyme expression in mutants are likely attributed to metabolic cues, such as serum glucose levels, which tightly regulate hepatic lipid metabolism.[43]

We further investigate the expression of lipogenic and lipolytic enzymes in gWAT and BAT. In gWAT, there was a reduction in ACC expression at ZT0 in mutant females (Figure S3C) similar to what was observed in the liver (Figure 2G). Notably, mutants also exhibited decreased ACC expression at ZT12, similar to controls (Figure S3C). However, no significant changes were observed in FAS and phosphorylated HSL expression (Figure S3C). The altered ACC expression in gWAT of mutant females was not associated with changes in BMAL1 expression (Figure S3C). Interestingly, in BAT, ACC expression was increased in mutants at ZT0 compared with controls, while the expression of other enzymes remained unaffected (Figure S3C).

Leptin, a hormone primarily produced in WAT, plays a crucial role in regulating feeding, body mass, and energy balance.[44] Controls exhibited higher leptin levels at ZT12 compared with ZT0 [45,46] (Figure S3D). In contrast, female mutants displayed elevated leptin levels at ZT0 (Figure S3D), which may be associated with reduced daytime food intake, improved glucose tolerance, and increased BAT thermogenic activity.[47,48]

BMAL1 KD in astrocytes alters basal diurnal metabolic rate in a sex-dependent manner

We assessed the impact of astrocytic BMAL1 KD on energy expenditure in male and female animals 8 weeks after TM treatment. Female Bmal1cKD mice showed increased energy expenditure, O_2 consumption, and CO_2 production during the dark phase (Figures 3A–3D), consistent with their lower body weight and increased feeding during the active period. The respiratory quotient remained similar to controls (Figure 3B). Analysis of feeding cycles revealed an increased period and advanced acrophase in female *Bmal1cKD*s (Figures 3E–3G). Furthermore, female mutants displayed higher periodicity in energy expenditure and respiratory cycles, along with an advanced acrophase in energy expenditure (Figures 3F and 3G). These findings suggest that astrocytic BMAL1 regulates the period and phase of the feeding pattern in females and that the changes in basal metabolic rate remain phase locked to the feeding cycles in the presence of reduced astrocytic BMAL1.

In contrast, male mutants did not exhibit significant changes in the respiratory quotient, total energy expenditure, or respiratory cycles compared with controls (Figures S4A–S4D). However, they showed increased periodicity and delayed acrophase in cyclic energy expenditure, O_2 consumption, and spontaneous locomotor activity (Figures S4F, S4G, and S2C). Importantly, these changes were not associated with alterations in the feeding cycles, which exhibited significantly shorter periods (Figures S4E and S4F). Thus, unlike females, astrocytic BMAL1 may be necessary to align metabolic cycles with the feeding pattern specifically in males.

Astrocytic BMAL1 modulates the phase entrainment to feeding time

As astrocytes play a role in nutrient sensing, and BMAL1 KD in astrocytes alters the feeding pattern[17] (Figure 1B), we investigated the influence of astrocytic BMAL1 on phase entrainment to feeding time. Following 12 weeks of TM treatment, before

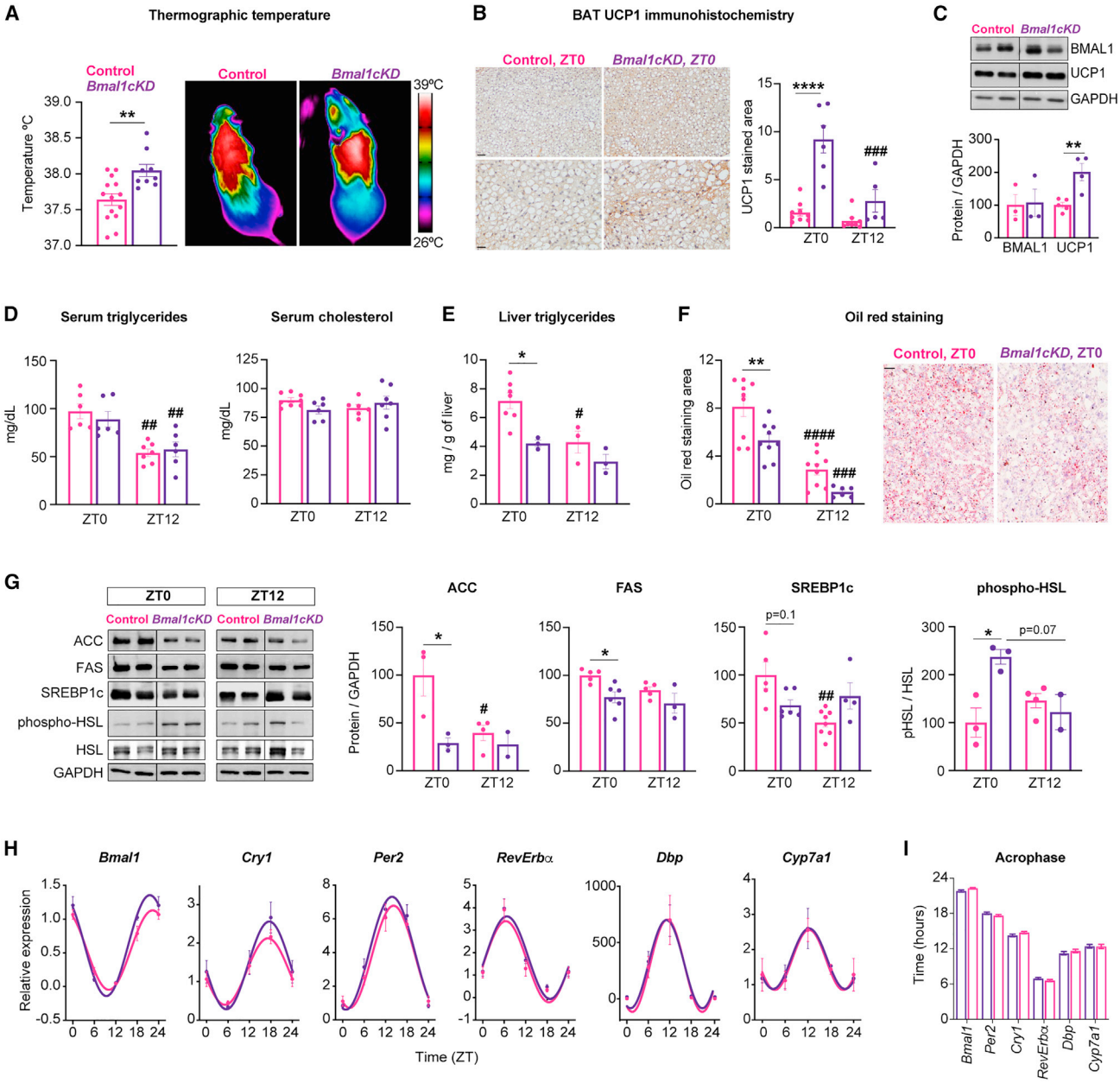

Figure 2. Astrocytic BMAL1 controls BAT thermogenesis and hepatic and WAT lipogenesis in females

(A) BAT temperature and thermal images of control and *Bmal1cKD*s 11 weeks after TM treatment (n = 9–14, paired t test, **p < 0.01).

(B) UCP1 BAT immunohistochemistry (n = 5–9, two-way ANOVA, ****p < 0.0001; ###p < 0.001 vs. ZT0). Scale bar: 10 μm (top images) and 20 μm (bottom images).

(C) BMAL1 and UCP1 BAT protein levels of control and mutants at ZT0 (n = 3–5, paired t test).

(D and E) Serum triglycerides and cholesterol (D) and liver triglycerides (E) in control and mutants 11 weeks after TM treatment (n = 3–10, two-way ANOVA, *p < 0.05; #p < 0.05 and ##p < 0.01 vs. ZT0).

(F) Liver oil red staining in control and *Bmal1cKDs* 11 weeks after TM treatment (n = 6–9, two-way ANOVA; ####p < 0.0001 vs. ZT0). Scale bar: 20 μm.

(G) Hepatic ACC, FAS, SREBP1c, phosphorylated (phospho-) HSL, and HLS expression of control and *Bmal1cKD*s 11 weeks after TM treatment (n = 2–4, two-way ANOVA).

(H and I) Hepatic clock genes and outputs (G) and obtained acrophase (I) in control and mutants after 10 weeks of TM treatment. Experimental data were cosine fitted (n = 4–6). Data are presented as mean ± SEM.

any dietary intervention, all animals exhibited standard nocturnal activity patterns, with no significant differences or increased activity observed before ZT4 (Figure 4A). We gradually reduced food availability to 6 h for 6 days (ZT4–ZT10) and further to 4 h for 4 days (ZT4–ZT8). During the restricted feeding (RF) period, food anticipatory activity (FAA) occurred 1 to 4 h before food

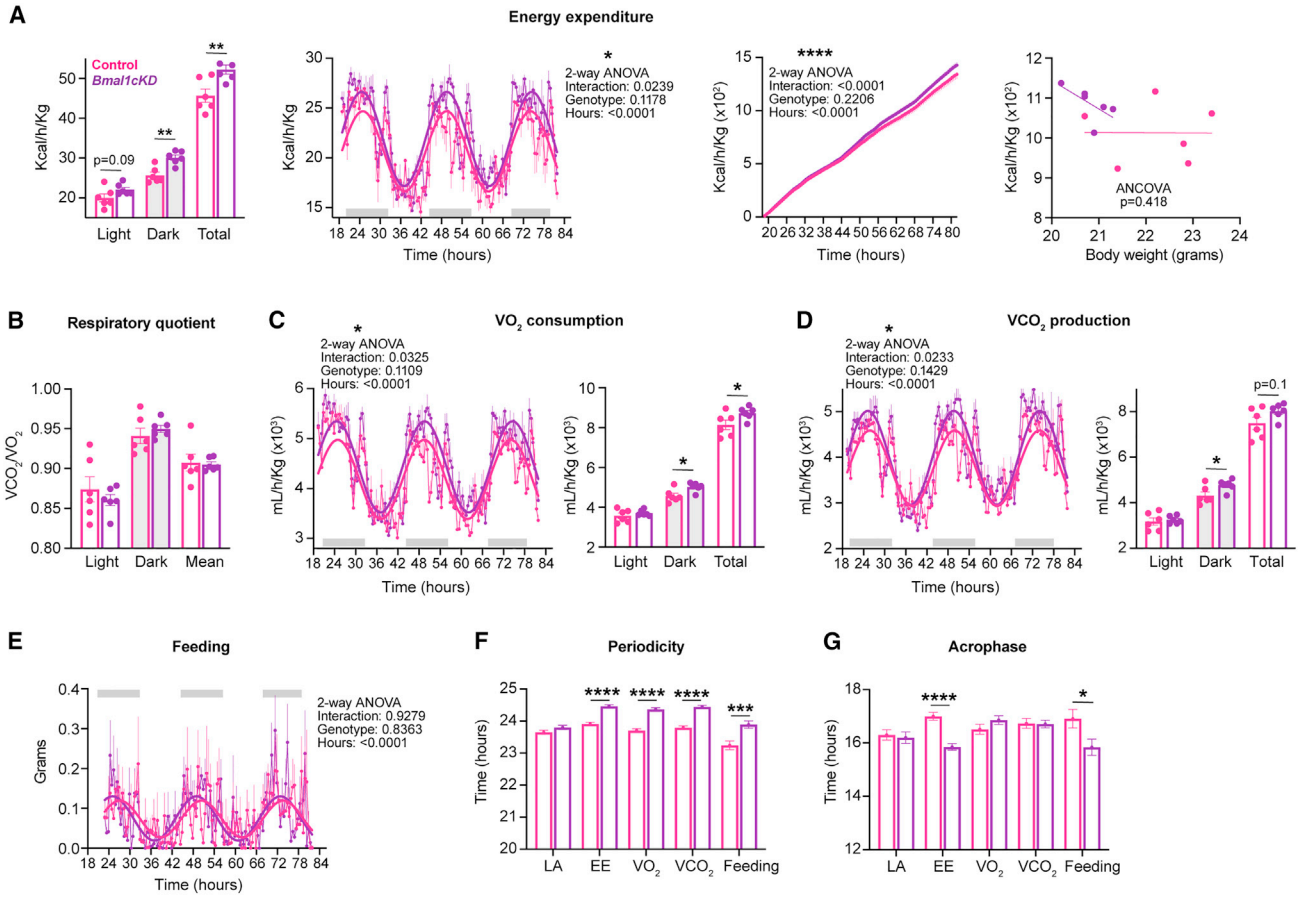

Figure 3. BMAL1 KD in astrocytes alters basal diurnal metabolic rate in a sex-dependent manner

(A, C, and D) Energy expenditure, O_2 consumption, and CO_2 production in control and *Bmal1cKD* females 8 weeks after TM treatment. Experimental data were cosine fitted (two-way ANOVA and paired t test, *p < 0.05, **p < 0.01, and ****p < 0.0001 vs. controls).

(B) Respiratory quotient in control and *Bmal1cKD* females.

(E) Feeding pattern of control and mutant females. Experimental data were cosine fitted.

(F and G) Periodicity (F) and acrophase (G) of spontaneous locomotor activity (LA), energy expenditure (EE), respiratory parameters, and feeding pattern in control and *Bmal1cKD* females (paired t test, ***p < 0.001). Data are presented as mean ± SEM (n = 5–6).

provision (Figures 4A and 4B). There was a significant decrease in nocturnal activity in males, whereas females exhibited a trend toward reduced activity that did not reach statistical significance (Figures 4A and 4C). However, the overall locomotor activity distribution and total activity remained similar between control and mutants (Figure 4D). Moreover, both male and female Bmal1cKDs exhibited similar acquisition of FAA compared with controls (Figures 4A, 4B, and 4E).[49,50]

Feeding schedules and caloric restriction advance the phase of nocturnal activity and the light-entrained rhythms of the SCN.[51,52] In line with this, control animals exhibited a significant phase advance of approximately 2 h in their nocturnal activity during the last 4 days of the RF compared with *ad libitum* conditions (Figure 4F). However, the phase advances were less pronounced in the mutants (Figure 4F), indicating that the requirement of astrocytic BMAL1 for SCN phase shifts in response to RF. Importantly, there were no differences in cumulative food intake (Figure 4G) or body weight (Figure 4H) between mutants and controls, suggesting that KD of astrocytic BMAL1 does not impact metabolic adaptation to RF.

Astrocytic BMAL1 differentially regulates energy balance in diet-induced obesity (DIO)

Consuming a high-fat diet (HFD) affects BMAL1 chromatin recruitment, thereby impacting metabolic pathways and clock genes.[53] To investigate the contribution of astrocytic BMAL1, we fed *Bmal1cKD* mice a 60% HFD for 16 weeks. Surprisingly, female DIO-challenged mutants showed increased body weight (Figure 5A) and food intake, particularly during the dark phase (Figures 5B and 5C), compared with controls. Notably, these females also showed increased fat deposits in the g, sc, and v regions, along with increased lean mass (Figure 5D). Thus, *Bmal1cKD* female mice exhibit a "male-like" pattern of fat distribution and body composition when exposed to an HFD. Further analysis revealed unchanged BAT thermogenesis (Figure 5E), but mutants exhibited reduced glucose tolerance (Figure 5F)

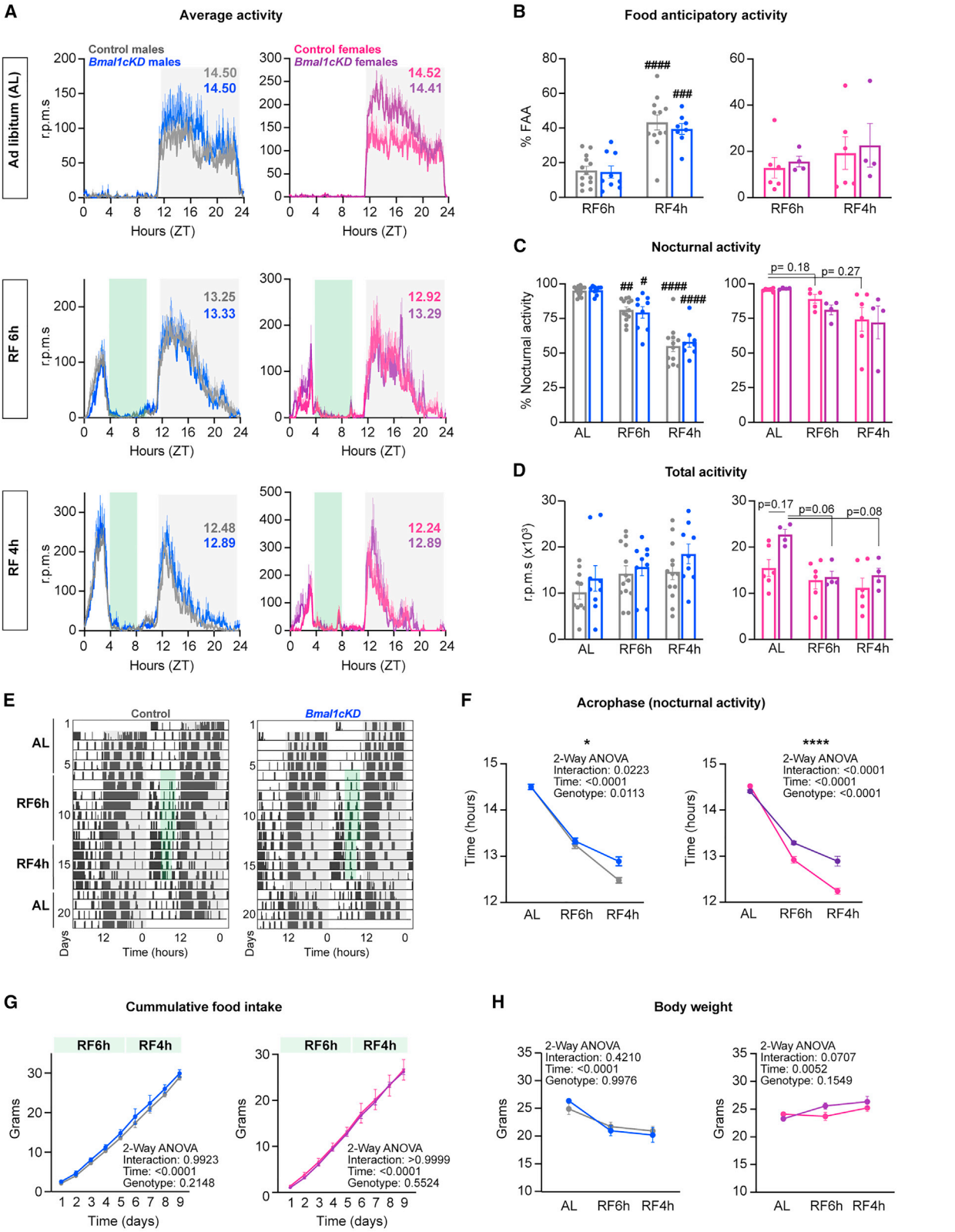

(legend on next page)

without altered INS sensitivity (Figure 5G). These effects were not attributed to differences in hypothalamic BMAL1 expression between DIO-challenged control mice and mutants (Figure S5A).

To further explore the metabolic effects of an HFD on *Bmal1cKD* females, we examined hepatic lipid metabolism, specifically focusing on liver lipogenesis. Mutants exhibited elevated serum triglyceride levels at ZT0, while their cholesterol levels were comparable to those of controls (Figure 5H). Interestingly, they showed reduced hepatic fat content at ZT12 (Figure 5I). Analysis of hepatic lipogenic enzyme expression revealed notable differences between DIO-challenged controls and mutants. Control mice on an HFD exhibited reduced ACC expression at ZT0 and FAS at both ZT0 and ZT12 compared with those on an STD (Figure S5B). In contrast, *Bmal1cKD* females displayed reduced ACC expression throughout the day and FAS at ZT12 (Figure S5B). However, there were no differences in SREBP1c expression between *Bmal1cKD* mice on an STD or an HFD (Figure S5B). Additionally, DIO-challenged *Bmal1cKD* females tended to show lower FAS expression compared with controls (Figure 5J), which correlated with their lower hepatic fat levels (Figure 5I). Importantly, the suppression of hepatic BMAL1 at ZT12 by the HFD was similar in control and mutants (Figure 5J), indicating that the expression of lipogenic enzymes was not influenced by differences in BMAL1 expression. These findings suggest that astrocytic BMAL1 promotes hepatic lipid storage in females independently of body weight.

Next, we investigated the impact of exposure to an HFD on the metabolic rate of *Bmal1cKO* females. Surprisingly, DIO-challenged mutants displayed reduced daily activity (Figure 6A) and energy expenditure (Figure 6B). They also showed a higher respiratory quotient (Figure 6C), indicating decreased utilization of dietary fat as a fuel source. These changes may contribute to their heightened susceptibility to the obesogenic effects of the HFD. Interestingly, the mutants displayed reduced periodicity in energy expenditure and respiratory parameters (Figures 6D–6F), suggesting disrupted energy utilization as an adaptive response to misalignment. Additionally, we observed an unexpected delay in the acrophase of their circadian locomotor activity (Figures 6A and 6F). These findings indicate that DIO partly mitigates certain metabolic consequences of BMAL1 KD in female astrocytes, as evidenced by the reduced energy expenditure and O_2 consumption observed in DIO-challenged *Bmal1cKD* mice.

Moving on to male mutants challenged with DIO, their body weight remained similar to controls (Figure S5C), but they exhibited increased food intake (Figures S5D and S5E). There were no significant changes in body composition, BAT temperature, serum cholesterol and triglycerides levels, or glucose tolerance (Figures S5F–S5I). Notably, male mutants showed increased INS sensitivity (Figure S5J). Moreover, their spontaneous activity, energy expenditure, respiratory quotient, O_2 consumption, or CO_2 production were comparable to controls (Figures S6A–S6E). Cosinor analysis of their locomotor activity, energy expenditure, and respiratory cycle curves revealed that the mutants exhibited significantly shorter rhythmic cycles (Figures S6A–S6F) and an advanced acrophase (Figures S6A–S6F) compared to the controls. These findings demonstrate that BMAL1 KD in astrocytes regulates energy balance in DIO in a sex-dependent manner.

Remarkably, the weight curve of Bmal1cKD females under HFD closely resembled that of male Bmal1cKD and control mice fed the same HFD (Figure S6G). Moreover, control females exhibited a more substantial drop in respiratory quotient compared with males when exposed to the HFD (Figure S6H), indicating their better regulation of energy balance and lower adiposity. Interestingly, the decrease in respiratory quotient in DIO-challenged Bmal1cKD females mirrored that of males under HFD (Figure S6H). Additionally, the increased body weight in DIO-challenged female mutants was primarily due to higher lean mass and heavier sc, v, and g fat pads (Figure 5D). These findings further support the notion that female Bmal1cKDs exhibit a ''male-like'' metabolic obese phenotype on an HFD, while male mutants develop obesity even on an STD.

Hypothalamic astrocytic BMAL1 regulates energy balance in a sex-dimorphic fashion

The mediobasal hypothalamus (MBH), consisting of the ARC and the ventromedial nucleus (VMH), plays a critical role in regulating energy balance.[54] The VMH integrates information from light exposure and nutrient availability, while the ARC contains an SCN-independent oscillator sensitive to feeding states.[55,56] However, the involvement of MBH astrocytic BMAL1 in cyclic energy homeostasis remains unclear. To investigate this, we employed a viral-mediated Cre/lox system[57–60] to selectively knock down BMAL1 in astrocytes within the MBH of the adult male or female *Bmal1*$^{fl/fl}$ mice (GFAP-Bmal1-KD). Successful Cre recombination was confirmed by GFP labeling, indicating specific targeting of astrocytes within the infected area of the hypothalamus in GFAP-*Bmal1*-KD mice (Figure 7A). Moreover, these mice exhibited a significant 40% decrease in BMAL1 protein levels in the MBH (Figure 7A).

Female GFAP-*Bmal1*-KD mice exhibited reduced body weight (Figure 7B) and a trend toward decreased adiposity and lean mass (Figure 7B). This was accompanied by significantly

Figure 4. Astrocytic BMAL1 modulates the phase entrainment to feeding time

(A) Average waveforms of control and *Bmal1cKD* mice under *ad libitum* (AL) conditions and during RF from ZT4 to ZT10 (RF6) or ZT4 to ZT8 (RF 4 h). Acrophase is indicated.

(B) FAA in control and mutants (two-way ANOVA, ###p < 0.001 and ####p < 0.0001 vs. RF 6 h).

(C and D) Nocturnal activity (C) and total activity (D) in control and *Bmal1cKDs* under AL and the RF paradigm (two-way ANOVA, #p < 0.05, ##p < 0.01, and ####p < 0.0001 vs. AL animals).

(E) Representative actograms of male control and *Bmal1cKD*s.

(F) Acrophase of nocturnal LA of control and *Bmal1cKD*s (*p < 0.05 and ****p < 0.0001).

(G and H) Cumulative food intake (G) and BWs (H) of control and mutants. Green areas indicate the feeding time, and gray areas indicate the nighttime. Data presented as mean ± SEM (n = 4–12).

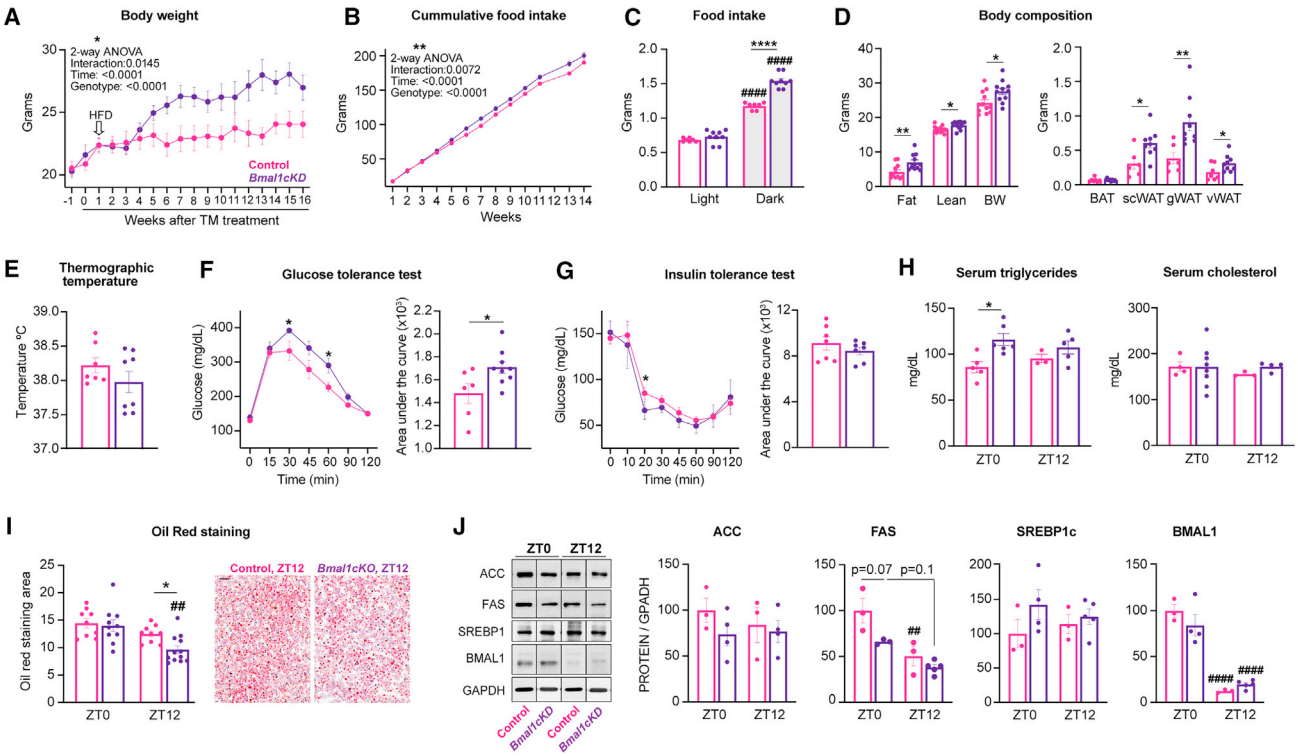

Figure 5. Astrocytic BMAL1 regulates peripheral metabolism in diet-induced obesity (DIO)-challenged females

(A) Age-dependent changes in BW of DIO-challenged control and mutants (n = 7–9, *p < 0.05).

(B) Cumulative food intake of DIO-challenged control and Bmal1cKDs (n = 7–9, **p < 0.01).

(C) Food intake after 4 weeks of HFD (n = 7–9, two-way ANOVA, ****p < 0.0001 and ####p < 0.0001 vs. daytime).

(D) Left: fat and lean mass of control and *Bmal1cKD*s after 14 weeks of HFD (BW). Right: weight of BAT, scWAT, gWAT, and vWAT after 15 weeks of HFD (n = 6–9, paired t test).

(E) BAT thermographic temperature after 8 weeks of HFD (n = 7–8).

(F and G) GTT (F) and ITT (G) in control and mutants after 6–7 weeks of HFD, performed at ZT10 (n = 6–9, paired t test).

(H and I) Serum triglycerides and cholesterol (H) and liver oil red staining (I) in control and *Bmal1cKD* females after 15 weeks of HFD (n = 3–12, two-way ANOVA, ##p < 0.01 vs. ZT0). Scale bar, 20 μm.

(J) Hepatic ACC, FAS, SREBP1c, and BMAL1 in DIO-challenged control and mutants for 15 weeks (n = 3–4, two-way ANOVA, ####p < 0.0001 vs. ZT0). Data are presented as mean ± SEM.

decreased food intake (Figure 7C), increased BAT thermogenesis (Figure 7D), and improved glucose tolerance (Figure 7E). The observed phenotype closely resembled that of *Bmal1cKD* females, except for decreased nighttime food intake. GFAP-*Bmal1*-KD females also showed enhanced glucose-stimulated INS secretion compared with controls (Figure 7E) and reduced liver triglyceride levels (Figure 7F), similar to *Bmal1cKD* mice. Importantly, BMAL1 KD in MBH astrocytes did not affect spontaneous activity (Figure 7G) but did increase energy expenditure (Figure 7H). The respiratory quotient in GFAP-*Bmal1*-KD females was comparable to controls (Figure 7I), while there was a significant increase in O_2 consumption and CO_2 production (Figures 7J and 7K). Although GFAP-*Bmal1*-KD females did not exhibit altered periodicity of metabolic cycles as observed in *Bmal1cKD* females, they did show an advanced acrophase of energy expenditure and feeding pattern (Figures 7L and 7M). Therefore, MBH astrocytic BMAL1 controls the phase of the feeding pattern, influencing basal metabolic and respiratory cycles in females.

In contrast, GFAP-*Bmal1*-KD males did not exhibit changes in body weight or composition (Figure S7A) but did show increased daytime food intake (Figure S7B)[17] and improved glucose tolerance, consistent with the findings in *Bmal1cKD* mice (Figure S7C).[17] Importantly, spontaneous activity, respiratory quotient, energy expenditure, and respiratory and feeding cycles were largely unaffected in male GFAP-*Bmal1*-KO mice (Figures S7D–S7J). These findings underscore the sex-dependent role of hypothalamic BMAL1 in energy balance and rhythmic energy expenditure.

To investigate the role of hypothalamic astrocytes more specifically, we targeted astrocytes in the ARC and selectively knocked down BMAL1 using a viral-mediated Cre/lox system approach.[57–60] The successful targeting of ARC astrocytes was confirmed by GFP labeling, which demonstrated specific infection within the hypothalamus in ARC-*Bmal1*-KD mice (Figure S7K). These mice exhibited a significant decrease in BMAL1 within the ARC (Figure S7K) and a substantial reduction in BMAL1-positive astrocytes (Figure S7L), similar to previous

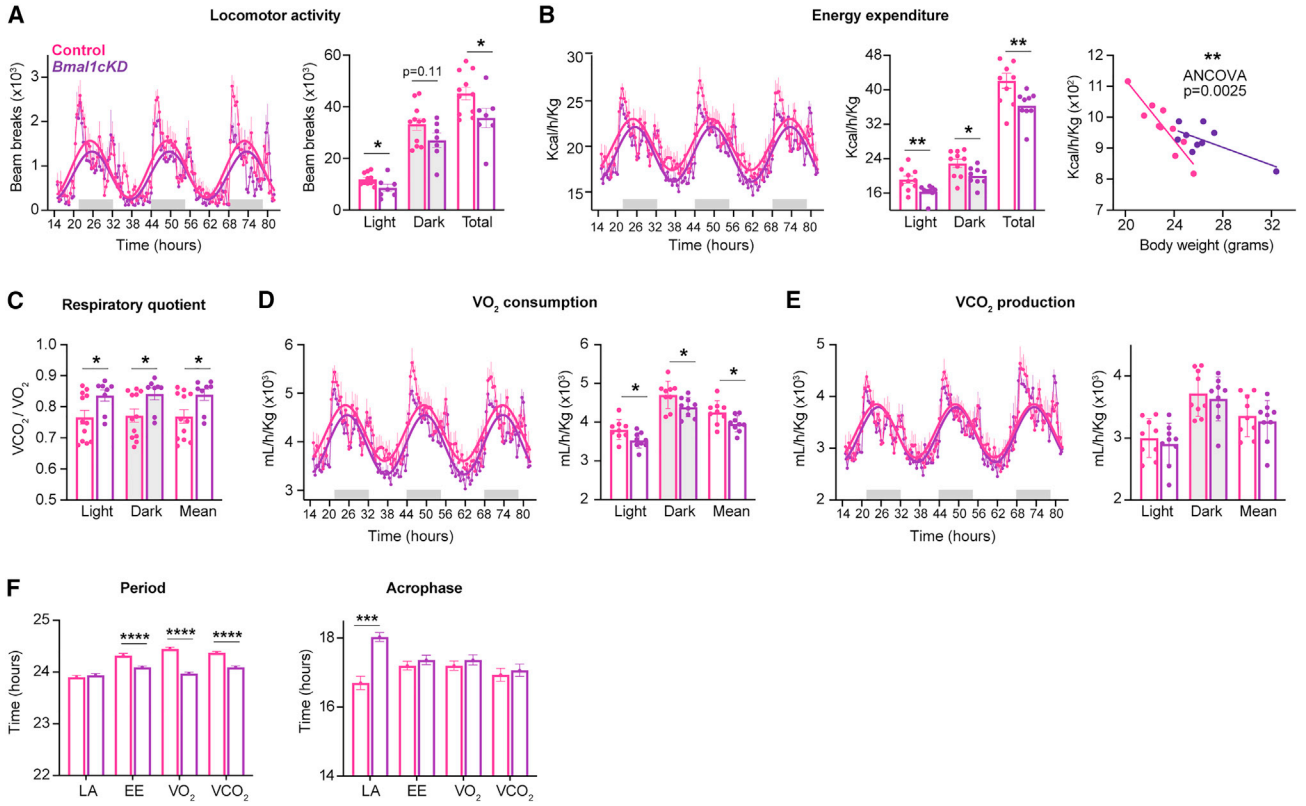

Figure 6. BMAL1 KD in female astrocytes regulates basal metabolic rate in obesity

(A, B, D, and E) LA, EE, O_2 consumption, and CO_2 production in DIO-challenged control and *Bmal1cKD* females for 11 weeks. Experimental data were cosine fitted (paired t test, *p < 0.05 and **p < 0.01).

(C) Respiratory quotient in DIO-challenged mice (paired t test).

(F) Periodicity and acrophase of activity, EE, and respiratory parameters in DIO-challenged control and mutants (paired t test, ***p < 0.01 and ****p < 0.0001). Data are presented as mean ± SEM (n = 7–11).

findings in *Bmal1cKD* mice (Barca-Mayo et al., 2020). Interestingly, ARC-*Bmal1*-KD mice showed normal body weight, composition, and glucose tolerance (Figures S7M–S7O). However, they did exhibit a notable reduction in food intake (Figure S7P). Thus, astrocytic BMAL1 within the ARC does not replicate the phenotypic changes observed in mice with BMAL1-deletion MBH or *Bmal1cKD* males. This highlights the specificity of astrocytic BMAL1 in different hypothalamic nuclei in regulating energy homeostasis and suggests the potential involvement of VMH astrocytes in controlling energy balance.

DISCUSSION

Considerable evidence from humans and rodent studies suggests a strong association between circadian disruption and metabolic disorders, as well as energy imbalance.[3,4,17,61,62] Recent research indicates gender differences in the metabolic consequences of circadian disruption.[23,63] However, the regulatory circuits involved and their gender-specific effects are not well understood. In our study, we found an unexpected role of MBH astrocytic BMAL1 in controlling energy expenditure, BAT function, and lipogenesis in the liver and WAT, with sex-dependent effects. Knocking down BMAL1 selectively in astrocytes amplified the metabolic differences between male and female mice on an STD. Conversely, loss of BMAL1 in female astrocytes resulted in a "male-like" metabolic obese phenotype when exposed to an HFD, likely due to reduced activity and energy expenditure and an elevated respiratory quotient. Thus, our findings propose that astrocytic BMAL1 plays a crucial role in sex-specific regulation of circadian clockwork, connecting it to metabolic outputs and physiological rhythms.

Male SCN astrocytes exhibit daily rhythms that determine the free-running period and the onset of wheel-running activity after transitioning from DD to a new LD cycle.[7,8,11] In contrast, female Bmal1cKD mice show normal locomotor behavior during free running, indicating that their central pacemaker is not intrinsically impaired. While BMAL1 recombination percentages in male and female SCN astrocytes are similar, incomplete BMAL1 recombination or specificity in females may explain their intact circadian locomotor behavior. Partial deletion of BMAL1[64,65] or partial lesions of the SCN[66–71] did not lead to the loss of rhythms. However, global disruption of the neuronal clock occurs when BMAL1 is deleted in a subset of astrocytes in both male[11,17] and female brains (present study), suggesting that a small number of astrocytes in the SCN can establish and sustain circadian patterns of activity and behavior.[10] The sex differences in

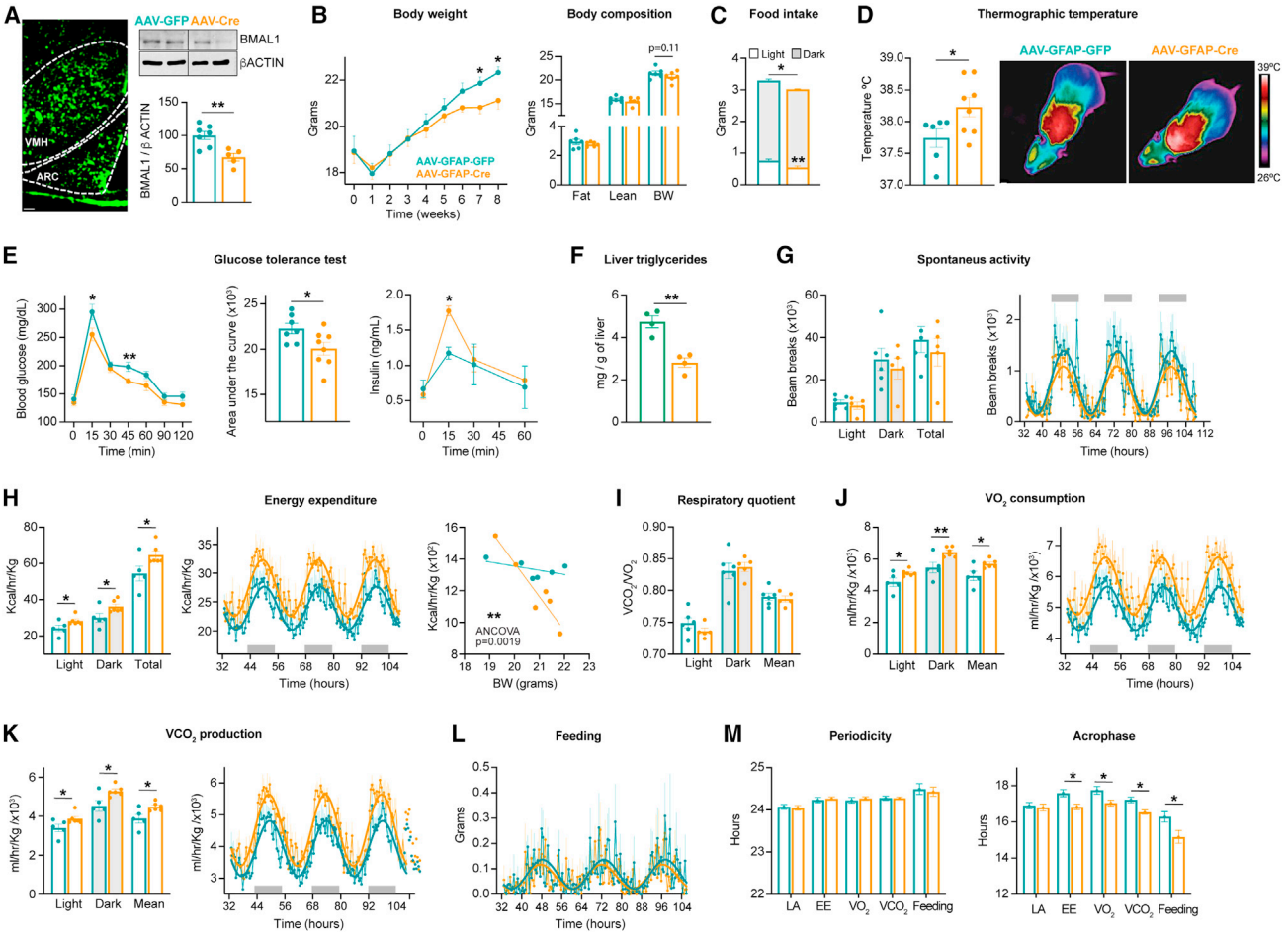

Figure 7. Hypothalamic astrocytic BMAL1 regulates energy balance in females

(A) Left: MBH showing adeno-associated virus (AAV)-GFAP-GFP infection in *Bmal1*$^{fl/fl}$ mice. Scale bar: 100 μm. Right: MBH BMAL1 expression of AAV-GFAP-GFP (controls) or AAV-GFAP-Cre (GFAP-*Bmal1*-KD) mice (n = 5–7, paired t test, **p < 0.01).

(B) Age-dependent BW changes and body composition of control and GFAP-*Bmal1*-KD mice after 8 weeks of AAV injection (n = 6–13, two-way ANOVA, *p < 0.05).

(C) Food intake in control and mutants after 6 weeks of AAV injection (n = 7–8, paired t test, **p < 0.01 vs. controls).

(D) BAT temperature and thermal images after 9 weeks of AAV injection (n = 6–8, paired t test).

(E) GTT and glucose-stimulated plasma insulin levels in control and mutants after 6 weeks of AAV injection, performed at ZT10 (n = 7–8, paired t test).

(F) Liver triglycerides after 10 weeks of AAV injection (n = 4, paired t test).

(G, H, J, and K) LA, EE, O_2 consumption, and CO_2 production in control or GFAP-*Bmal1*-KDs. Experimental data were cosine fitted (n = 5–6; paired t tests).

(I) Respiratory quotient in control and GFAP-*Bmal1*-KDs (n = 5–6).

(L) Feeding pattern in control and GFAP-*Bmal1*-KD females. Experimental data were cosine fitted (n = 5–6).

(M) Period and acrophase of LA, EE, respiratory parameters, and feeding cycles in control and female GFAP-*Bmal1*-KD (n = 5–6; paired t test). Data presented as mean ± SEM.

circadian locomotor activity of *Bmal1cKD* mice align with previous findings indicating enhanced adaptability and resilience in female mice to phase shifts and circadian disruptions.[25] Male rodents, on the other hand, demonstrate a greater ability to maintain entrainment compared with females.[22] Further investigation is needed to determine the role of BMAL1 in SCN astrocytes in regulating energy balance and peripheral metabolism in females. However, targeting all astrocytes *in vivo* is challenging due to their widespread distribution and their region-specific gene expression. Nonetheless, our study demonstrates that deleting BMAL1 in MBH astrocytes partially replicates the metabolic phenotype observed in female *Bmal1cKD*s, including reduced body weight, altered cyclic energy expenditure, BAT thermogenesis, glucose tolerance, and liver triglyceride levels. It is important to note that differences between Glast-*Bmal1* global astrocyte KD and GFAP-*Bmal1* hypothalamic KD phenotypes may arise from the use of different Cre drivers.

Our comprehensive characterization of the metabolic phenotype in Bmal1cKD mutants reveals that astrocytic BMAL1 influences energy expenditure in a sex-dependent manner. This finding aligns with a previous study demonstrating sex-specific effects of circadian misalignment on energy utilization.[23] In

females, circadian misalignment leads to reduced carbohydrate oxidation rate and respiratory quotients, along with increased energy expenditure and lipid oxidation rate.[23] Similarly, our results indicate that knocking down astrocytic BMAL1 increases BAT thermogenesis and energy expenditure in females. Interestingly, we observed that female mutants demonstrate resilience in synchronizing their cyclic energy expenditure with the feeding patterns, while in males, metabolic cycles are synchronized with spontaneous circadian activity. This suggests a potential interaction between the effects of astrocytic BMAL1 KD on metabolic dysfunctions in males and SCN-mediated rhythms. Thus, it is reasonable to hypothesize that astrocytes integrate light and nutrient inputs and establish connections between the SCN and other circuits to optimize energy balance in males.

Importantly, the over-activation of BAT in Bmal1cKD females mainly occurs during the dark period, indicating a circadian component in these effects. Interestingly, we did not observe differences in BMAL1 expression in the BAT of female mutants at the beginning of the light and dark phases. However, we did find that the SNS plays a role in triggering BAT over-activation in female mutants. Additionally, KD of BMAL1 in astrocytes of the MBH in females is sufficient to modulate cyclic energy expenditure and BAT thermogenesis. Thus, our findings provide strong evidence that, in addition to neuronal control,[56,72] astrocytic BMAL1 regulates BAT thermogenesis, likely through its influence on the circadian regulation of the SNS. Furthermore, our observations reveal an interesting trend: mutants show increased *de novo* FAS in BAT. This increased synthesis may serve as a mechanism to generate fuel for enhanced thermogenesis, compensating for the reduced availability of free fatty acids from the liver and WAT. Indeed, sympathetic activation of β-ARs during cold exposure is known to stimulate both *de novo* FAS and oxidation in BAT.[73]

The well-established inverse correlation between the presence of brown and beige adipocytes and the development of obesity and type 2 diabetes in humans is widely recognized.[74] Importantly, loss of astrocytic BMAL1 improves glucose tolerance in both males and females. However, it is noteworthy that only female mutants exhibited increased BAT stimulation, suggesting that the primary factors contributing to improved glucose tolerance in females are likely heightened BAT thermogenesis (resulting in enhanced glucose clearance) and increased INS secretion. This highlights the presence of sex-specific mechanisms in the integration of BAT function and glucose homeostasis.

Further research is needed to elucidate the precise mechanisms underlying the sex-dependent control of energy balance by astrocytic BMAL1 in both chow and HFD conditions. However, several possibilities can be speculated. (1) Our findings suggest that astrocytic BMAL1 might integrate ovarian estrogen (E2) signaling differently in chow and HFD. It is possible that astrocytic BMAL1 converges E2 signaling with neuroendocrine stimuli associated with HFD, potentially involving increased leptin levels, to maintain energy homeostasis in a hypercaloric environment.[75,76] This could be related to the regulation of estrogen receptor β expression by BMAL1,[77] enhancing the ability of E2 to decrease food intake in the presence of hyperleptinemia. (2) Astrocytic BMAL1 may utilize distinct molecular pathways to regulate gene expression and physiological rhythms in males and females. Consequently, KD of astrocytic BMAL1 in females could disrupt the coordination between peripheral functions in the liver, BAT, and WAT and feeding/metabolic rhythms, particularly in response to HFD. Investigating the rhythmic outputs from astrocytes to various peripheral axes, such as adipose tissues and the liver, and how they integrate endocrine signals controlling energy balance in males and females will pose challenges for future studies. Understanding the sex differences in these circadian mechanisms is crucial for comprehending the divergent responses to circadian disruption[23,78–80] and other sex dimorphisms. Our findings provide valuable insights into the potential development of gender-specific treatments for diseases related to cellular clocks, energy homeostasis, and peripheral metabolism, providing opportunities for designing chronotherapeutic strategies.

Limitations of the study

Our study has certain limitations that should be acknowledged. Firstly, while our findings do not strongly support the direct involvement of astrocytic BMAL1 in circadian locomotor behavior or metabolic adaptation to the RF, it is important to consider that a partial reduction of astrocytic BMAL1 or the presence of BMAL1 in specific brain regions may still have functional implications. Further investigations using a complete knockout of astrocytic BMAL1 or alternative methods to modulate its expression will provide more insights into its precise contributions to these processes.

Additionally, caution should be exercised when interpreting our results regarding lipogenesis in the liver, gWAT, and BAT, as the analysis was limited by the small number of samples profiled. However, we observed significant trends that were supported by the assessment of liver triglycerides and oil red staining. These findings suggest that there may be an upregulation in *de novo* FAS as a potential compensatory mechanism to generate fuel for heightened thermogenesis, considering the reduced availability of free fatty acids from the liver and WAT. Although the findings are limited by the small sample size, they provide valuable insights into the metabolic phenotypes of the mutants.

STAR★METHODS

Detailed methods are provided in the online version of this paper and include the following:

- KEY RESOURCES TABLE
- RESOURCE AVAILABILITY
  - Lead contact
  - Materials availability
  - Data and code availability
- EXPERIMENTAL MODEL AND STUDY PARTICIPANT DETAILS
  - Animals
- METHOD DETAILS
  - Treatments
  - Determination of the body composition
  - Thermographic temperature

- Indirect calorimetry
- Ovariectomy
- Stereotaxic microinjections of AAV
- Open field test
- Circadian locomotor activity
- Food restriction experiments
- Glucose and insulin tolerance test
- Glucose-stimulated insulin secretion
- Determination of metabolic markers
- Immunofluorescence
- RNA isolation and quantitative RT-PCR
- Western blotting
- Histological analysis

- QUANTIFICATION AND STATISTICAL ANALYSIS

SUPPLEMENTAL INFORMATION

Supplemental information can be found online at https://doi.org/10.1016/j.celrep.2023.112949.

ACKNOWLEDGMENTS

This work was supported by Xunta de Galicia (Consellería de Cultura, Educación e Ordenación Universitaria) (O.B.-M.: ED431F 2020/009); the Agencia Estatal de Investigación (O.B.-M.: PID2019-109556RB-I00); the Ministerio de Ciencia e Innovación (M.L.: PID2021-128145NB-I00 and PDC2022-133958-I00); the "la Caixa" Foundation (M.L.: ID 100010434); and Xunta de Galicia support for CiMUS (2016–2019, ED431G/05). O.B.-M. received a Ramón y Cajal award (RYC2018-026293-I) from the Spanish Ministerio de Ciencia, Innovación y Universidades. M.L.-M. and M.S.-L. are supported by the Ministerio de Ciencia, Innovación y Universidades of Spain (PRE2020-093614 and FPU2018/00647).

AUTHOR CONTRIBUTIONS

In vivo experiments, M.L.-M., A.G.-V., A.E.-S., M.S.-L., and N.R.V.D.; tissue analysis, M.L.-M., N.O., P.N.-R., and M.G.-D.; methodology, M.L.-M.; review & editing, all authors; experiment design, writing, and funding acquisition, O.B.-M. and M.L.; conceptualization, formal analysis, and supervision, O.B.-M.

DECLARATION OF INTERESTS

The authors declare no competing interests.

Received: July 1, 2022
Revised: June 12, 2023
Accepted: July 20, 2023
Published: August 4, 2023

REFERENCES

1. Myers, M.G., Jr., and Olson, D.P. (2012). Central nervous system control of metabolism. Nature *491*, 357–363. https://doi.org/10.1038/NATURE11705.
2. López, M. (2022). Hypothalamic AMPK as a possible target for energy balance-related diseases. Trends Pharmacol. Sci. *43*, 546–556. https://doi.org/10.1016/J.TIPS.2022.04.007.
3. Eckel-Mahan, K., and Sassone-Corsi, P. (2013). Metabolism and the circadian clock converge. Physiol. Rev. *93*, 107–135. https://doi.org/10.1152/PHYSREV.00016.2012.
4. Barca-Mayo, O., and López, M. (2021). Astrocyte Clocks and Glucose Homeostasis. Front. Endocrinol. *12*, 662017. https://doi.org/10.3389/FENDO.2021.662017/ENDNOTE.
5. Moore, R.Y., and Eichler, V.B. (1972). Loss of a circadian adrenal corticosterone rhythm following suprachiasmatic lesions in the rat. Brain Res. *42*, 201–206. https://doi.org/10.1016/0006-8993(72)90054-6.
6. Stephan, F.K., and Zucker, I. (1972). Circadian rhythms in drinking behavior and locomotor activity of rats are eliminated by hypothalamic lesions. Proc. Natl. Acad. Sci. USA *69*, 1583–1586. https://doi.org/10.1073/pnas.69.6.1583.
7. Brancaccio, M., Patton, A.P., Chesham, J.E., Maywood, E.S., and Hastings, M.H. (2017). Astrocytes Control Circadian Timekeeping in the Suprachiasmatic Nucleus via Glutamatergic Signaling. Neuron *93*, 1420–1435.e5. https://doi.org/10.1016/J.NEURON.2017.02.030.
8. Tso, C.F., Simon, T., Greenlaw, A.C., Puri, T., Mieda, M., and Herzog, E.D. (2017). Astrocytes Regulate Daily Rhythms in the Suprachiasmatic Nucleus and Behavior. Curr. Biol. *27*, 1055–1061. https://doi.org/10.1016/j.cub.2017.02.037.
9. Barca Mayo, O., Berdondini, L., and De Pietri Tonelli, D. (2019). Methods in Molecular Biology vol 1938. In Astrocytes and Circadian Rhythms: An Emerging Astrocyte–Neuron Synergy in the Timekeeping System (Humana Press). https://doi.org/10.1007/978-1-4939-9068-9_10.
10. Brancaccio, M., Edwards, M.D., Patton, A.P., Smyllie, N.J., Chesham, J.E., Maywood, E.S., and Hastings, M.H. (2019). Cell-autonomous clock of astrocytes drives circadian behavior in mammals. Science *363*, 187–192. https://doi.org/10.1126/science.aat4104.
11. Barca-Mayo, O., Pons-Espinal, M., Follert, P., Armirotti, A., Berdondini, L., and De Pietri Tonelli, D. (2017). Astrocyte deletion of Bmal1 alters daily locomotor activity and cognitive functions via GABA signalling. Nat. Commun. *8*, 14336. https://doi.org/10.1038/ncomms14336.
12. Pezük, P., Mohawk, J.A., Wang, L.A., and Menaker, M. (2012). Glucocorticoids as entraining signals for peripheral circadian oscillators. Endocrinology *153*, 4775–4783. https://doi.org/10.1210/en.2012-1486.
13. Crosby, P., Hamnett, R., Putker, M., Hoyle, N.P., Reed, M., Karam, C.J., Maywood, E.S., Stangherlin, A., Chesham, J.E., Hayter, E.A., et al. (2019). Insulin/IGF-1 Drives PERIOD Synthesis to Entrain Circadian Rhythms with Feeding Time. Cell *177*, 896–909.e20. https://doi.org/10.1016/j.cell.2019.02.017.
14. Asher, G., and Sassone-Corsi, P. (2015). Time for food: The intimate interplay between nutrition, metabolism, and the circadian clock. Cell *161*, 84–92. https://doi.org/10.1016/j.cell.2015.03.015.
15. Orozco-Solis, R., and Sassone-Corsi, P. (2014). Circadian clock: linking epigenetics to aging. Curr. Opin. Genet. Dev. *26*, 66–72. https://doi.org/10.1016/J.GDE.2014.06.003.
16. Buxton, O.M., Pavlova, M., Reid, E.W., Wang, W., Simonson, D.C., and Adler, G.K. (2010). Sleep restriction for 1 week reduces insulin sensitivity in healthy men. Diabetes *59*, 2126–2133. https://doi.org/10.2337/db09-0699.
17. Barca-Mayo, O., Boender, A.J., Armirotti, A., and De Pietri Tonelli, D. (2020). Deletion of astrocytic BMAL1 results in metabolic imbalance and shorter lifespan in mice. Glia *68*, 1131–1147. https://doi.org/10.1002/GLIA.23764.
18. Sen, S., Dumont, S., Sage-Ciocca, D., Reibel, S., de Goede, P., Kalsbeek, A., and Challet, E. (2018). Expression of the clock gene Rev-erbα in the brain controls the circadian organisation of food intake and locomotor activity, but not daily variations of energy metabolism. J. Neuroendocrinol. *30*, e12557. https://doi.org/10.1111/jne.12557.
19. Paschos, G.K., Ibrahim, S., Song, W.L., Kunieda, T., Grant, G., Reyes, T.M., Bradfield, C.A., Vaughan, C.H., Eiden, M., Masoodi, M., et al. (2012). Obesity in mice with adipocyte-specific deletion of clock component Arntl. Nat. Med. *18*, 1768–1777. https://doi.org/10.1038/nm.2979.
20. Hasan, N., Nagata, N., Morishige, J.I., Islam, M.T., Jing, Z., Harada, K.I., Mieda, M., Ono, M., Fujiwara, H., Daikoku, T., et al. (2021). Brown adipocyte-specific knockout of Bmal1 causes mild but significant thermogenesis impairment in mice. Mol. Metabol. *49*, 101202. https://doi.org/10.1016/J.MOLMET.2021.101202.

21. Hatcher, K.M., Royston, S.E., and Mahoney, M.M. (2020). Modulation of circadian rhythms through estrogen receptor signaling. Eur. J. Neurosci. *51*, 217–228. https://doi.org/10.1111/EJN.14184.

22. Davis, F.C., Darrow, J.M., and Menaker, M. (1983). Sex differences in the circadian control of hamster wheel-running activity. Am. J. Physiol. *244*, R93–R105. https://doi.org/10.1152/AJPREGU.1983.244.1.R93.

23. Qian, J., Morris, C.J., Caputo, R., Wang, W., Garaulet, M., and Scheer, F.A.J.L. (2019). Sex differences in the circadian misalignment effects on energy regulation. Proc. Natl. Acad. Sci. USA *116*, 23806–23812. https://doi.org/10.1073/pnas.1914003116.

24. Karatsoreos, I.N., Butler, M.P., Lesauter, J., and Silver, R. (2011). Androgens modulate structure and function of the suprachiasmatic nucleus brain clock. Endocrinology *152*, 1970–1978. https://doi.org/10.1210/EN.2010-1398.

25. Alibhai, F.J., Reitz, C.J., Peppler, W.T., Basu, P., Sheppard, P., Choleris, E., Bakovic, M., and Martino, T.A. (2018). Female Clock Δ19/Δ19 mice are protected from the development of age-dependent cardiomyopathy. Cardiovasc. Res. *114*, 259–271. https://doi.org/10.1093/CVR/CVX185.

26. Riccitelli, S., Boi, F., Lonardoni, D., Giantomasi, L., Barca-Mayo, O., De Pietri Tonelli, D., Bisti, S., Di Marco, S., and Berdondini, L. (2022). Glial Bmal1 role in mammalian retina daily changes. Sci. Rep. *12*, 21561. https://doi.org/10.1038/S41598-022-25783-1.

27. Mori, T., Tanaka, K., Buffo, A., Wurst, W., Kühn, R., and Götz, M. (2006). Inducible gene deletion in astroglia and radial glia - A valuable tool for functional and lineage analysis. Glia *54*, 21–34. https://doi.org/10.1002/GLIA.20350.

28. Giantomasi, L., Ribeiro, J.F., Barca-Mayo, O., Malerba, M., Miele, E., De Pietri Tonelli, D., and Berdondini, L. (2023). Astrocytes actively support long-range molecular clock synchronization of segregated neuronal populations. Sci. Rep. *13*, 4815. https://doi.org/10.1038/S41598-023-31966-1.

29. MacCannell, A.D.V., Futers, T.S., Whitehead, A., Moran, A., Witte, K.K., and Roberts, L.D. (2021). Sexual dimorphism in adipose tissue mitochondrial function and metabolic flexibility in obesity. Int. J. Obes. *45*, 1773–1781. https://doi.org/10.1038/S41366-021-00843-0.

30. Yu, K., He, Y., Hyseni, I., Pei, Z., Yang, Y., Xu, P., Cai, X., Liu, H., Qu, N., Liu, H., et al. (2020). 17β-estradiol promotes acute refeeding in hungry mice via membrane-initiated ERα signaling. Mol. Metabol. *42*, 101053. https://doi.org/10.1016/J.MOLMET.2020.101053.

31. Dragano, N., Milbank, E., and López, M. (2020). Estradiol and Appetite: To Eat or Not to Eat, *42*, 101061. https://doi.org/10.1016/J.MOLMET.2020.101061.

32. Ludgero-Correia, A., Aguila, M.B., Mandarim-de-Lacerda, C.A., and Faria, T.S. (2012). Effects of high-fat diet on plasma lipids, adiposity, and inflammatory markers in ovariectomized C57BL/6 mice. Nutrition *28*, 316–323. https://doi.org/10.1016/J.NUT.2011.07.014.

33. Fernández-Murga, M.L., Vinué, Á., Ramón Caeiro, J., Guede, D., Tarín, J.J., Andrés, V., and Cano, A. (2015). Impact of estrogens on atherosclerosis and bone in the apolipoprotein E-deficient mouse model. Menopause *22*, 428–436. https://doi.org/10.1097/GME.0000000000000328.

34. Chiba, H., Uehara, M., Wu, J., Wang, X., Masuyama, R., Suzuki, K., Kanazawa, K., and Ishimi, Y. (2003). Hesperidin, a citrus flavonoid, inhibits bone loss and decreases serum and hepatic lipids in ovariectomized mice. J. Nutr. *133*, 1892–1897. https://doi.org/10.1093/jn/133.6.1892.

35. Lukowicz, C., Ellero-Simatos, S., Régnier, M., Oliviero, F., Lasserre, F., Polizzi, A., Montagner, A., Smati, S., Boudou, F., Lenfant, F., et al. (2019). Dimorphic metabolic and endocrine disorders in mice lacking the constitutive androstane receptor. Sci. Rep. *9*, 20169. https://doi.org/10.1038/S41598-019-56570-0.

36. Martini, T., Ripperger, J.A., Stalin, J., Kores, A., Stumpe, M., and Albrecht, U. (2021). Deletion of the clock gene Period2 (Per2) in glial cells alters mood-related behavior in mice. Sci. Rep. *11*, 12242. https://doi.org/10.1038/S41598-021-91770-7.

37. Kondratova, A.A., Dubrovsky, Y.V., Antoch, M.P., and Kondratov, R.V. (2010). Circadian clock proteins control adaptation to novel environment and memory formation. Aging (Albany. NY) *2*, 285–297. https://doi.org/10.18632/aging.100142.

38. Herrera Moro Chao, D., Kirchner, M.K., Pham, C., Foppen, E., Denis, R.G.P., Castel, J., Morel, C., Montalban, E., Hassouna, R., Bui, L.C., et al. (2022). Hypothalamic astrocytes control systemic glucose metabolism and energy balance. Cell Metabol. *34*, 1532–1547.e6. https://doi.org/10.1016/J.CMET.2022.09.002.

39. Gnocchi, D., Pedrelli, M., Hurt-Camejo, E., and Parini, P. (2015). Lipids around the Clock: Focus on Circadian Rhythms and Lipid Metabolism. Biol. *4*, 104–132. https://doi.org/10.3390/biology4010104.

40. Razzoli, M., Emmett, M.J., Lazar, M.A., and Bartolomucci, A. (2018). b-Adrenergic receptors control brown adipose UCP-1 tone and cold response without affecting its circadian rhythmicity. Faseb. J. *32*, 5640–5646. https://doi.org/10.1096/fj.201800452R.

41. Matsumoto, E., Ishihara, A., Tamai, S., Nemoto, A., Iwase, K., Hiwasa, T., Shibata, S., and Takiguchi, M. (2010). Time of day and nutrients in feeding govern daily expression rhythms of the gene for sterol regulatory element-binding protein (SREBP)-1 in the mouse liver. J. Biol. Chem. *285*, 33028–33036. https://doi.org/10.1074/JBC.M109.089391.

42. Shimizu, H., Hanzawa, F., Kim, D., Sun, S., Laurent, T., Umeki, M., Ikeda, S., Mochizuki, S., and Oda, H. (2018). Delayed first active-phase meal, a breakfast-skipping model, led to increased body weight and shifted the circadian oscillation of the hepatic clock and lipid metabolism-related genes in rats fed a high-fat diet. PLoS One *13*, e0206669. https://doi.org/10.1371/JOURNAL.PONE.0206669.

43. Grønning-Wang, L.M., Bindesbøll, C., and Nebb, H.I. (2013). Lipid Metabolism. IntechOpen. The Role of Liver X Receptor in Hepatic de novo Lipogenesis and Crosstalk with Insulin and Glucose Signaling. https://doi.org/10.5772/51357.

44. Friedman, J.M. (2019). Leptin and the endocrine control of energy balance. Nat. Metab. *1*, 754–764. https://doi.org/10.1038/s42255-019-0095-y.

45. Arble, D.M., Vitaterna, M.H., and Turek, F.W. (2011). Rhythmic leptin is required for weight gain from circadian desynchronized feeding in the mouse. PLoS One *6*, e25079. https://doi.org/10.1371/journal.pone.0025079.

46. Kettner, N.M., Mayo, S.A., Hua, J., Lee, C., Moore, D.D., and Fu, L. (2015). Circadian dysfunction induces leptin resistance in mice. Cell Metabol. *22*, 448–459. https://doi.org/10.1016/j.cmet.2015.06.005.

47. Commins, S.P., Marsh, D.J., Thomas, S.A., Watson, P.M., Padgett, M.A., Palmiter, R., and Gettys, T.W. (1999). Norepinephrine is required for leptin effects on gene expression in brown and white adipose tissue. Endocrinology *140*, 4772–4778. https://doi.org/10.1210/ENDO.140.10.7043.

48. Commins, S.P., Watson, P.M., Padgett, M.A., Dudley, A., Argyropoulos, G., and Gettys, T.W. (1999). Induction of uncoupling protein expression in brown and white adipose tissue by leptin. Endocrinology *140*, 292–300. https://doi.org/10.1210/ENDO.140.1.6399.

49. Pendergast, J.S., Nakamura, W., Friday, R.C., Hatanaka, F., Takumi, T., and Yamazaki, S. (2009). Robust Food Anticipatory Activity in BMAL1-Deficient Mice. PLoS One *4*, 4860. https://doi.org/10.1371/journal.pone.0004860.

50. Storch, K.F., and Weitz, C.J. (2009). Daily rhythms of food-anticipatory behavioral activity do not require the known circadian clock. Proc. Natl. Acad. Sci. USA *106*, 6808–6813. https://doi.org/10.1073/pnas.0902063106.

51. Holmes, M.M., and Mistlberger, R.E. (2000). Food anticipatory activity and photic entrainment in food restricted BALB/c mice. Physiol. Behav. *68*, 655–666. https://doi.org/10.1016/S0031-9384(99)00231-0.

52. Sen, S., Raingard, H., Dumont, S., Kalsbeek, A., Vuillez, P., and Challet, E. (2017). Ultradian feeding in mice not only affects the peripheral clock in the liver, but also the master clock in the brain. Chronobiol. Int. *34*, 17–36. https://doi.org/10.1080/07420528.2016.1231689.

53. Eckel-Mahan, K.L., Patel, V.R., De Mateo, S., Orozco-Solis, R., Ceglia, N.J., Sahar, S., Dilag-Penilla, S.A., Dyar, K.A., Baldi, P., and Sassone-Corsi, P. (2013). Reprogramming of the circadian clock by nutritional challenge. Cell *155*, 1464–1478. https://doi.org/10.1016/j.cell.2013.11.034.

54. Blanco, M.E., Mayo, O.B., Bandiera, T., De Pietri Tonelli, D., and Armirotti, A. (2020). LC–MS/MS analysis of twelve neurotransmitters and amino acids in mouse cerebrospinal fluid. J. Neurosci. Methods *341*, 108760. https://doi.org/10.1016/J.JNEUMETH.2020.108760.

55. Guilding, C., Hughes, A.T.L., Brown, T.M., Namvar, S., and Piggins, H.D. (2009). A riot of rhythms: neuronal and glial circadian oscillators in the mediobasal hypothalamus. Mol. Brain *2*, 28-19. https://doi.org/10.1186/1756-6606-2-28.

56. Orozco-Solis, R., Aguilar-Arnal, L., Murakami, M., Peruquetti, R., Ramadori, G., Coppari, R., and Sassone-Corsi, P. (2016). The circadian clock in the ventromedial hypothalamus controls cyclic energy expenditure. Cell Metabol. *23*, 467–478. https://doi.org/10.1016/j.cmet.2016.02.003.

57. Martínez-Sánchez, N., Seoane-Collazo, P., Contreras, C., Varela, L., Villarroya, J., Rial-Pensado, E., Buqué, X., Aurrekoetxea, I., Delgado, T.C., Vázquez-Martínez, R., et al. (2017). Hypothalamic AMPK–ER stress–JNK1 axis mediates the central actions of thyroid hormones on energy balance. Cell Metabol. *26*, 212–229.e12. https://doi.org/10.1016/j.cmet.2017.06.014.

58. Martínez de Morentin, P.B., González-García, I., Martins, L., Lage, R., Fernández-Mallo, D., Martínez-Sánchez, N., Ruíz-Pino, F., Liu, J., Morgan, D.A., Pinilla, L., et al. (2014). Estradiol regulates brown adipose tissue thermogenesis via hypothalamic AMPK. Cell Metabol. *20*, 41–53. https://doi.org/10.1016/j.cmet.2014.03.031.

59. González-García, I., Martínez de Morentin, P.B., Estévez-Salguero, Á., Contreras, C., Romero-Picó, A., Fernø, J., Nogueiras, R., Diéguez, C., Tena-Sempere, M., Tovar, S., and López, M. (2018). mTOR signaling in the arcuate nucleus of the hypothalamus mediates the anorectic action of estradiol. J. Endocrinol. *238*, 177–186. https://doi.org/10.1530/JOE-18-0190.

60. Contreras, C., González-García, I., Martínez-Sánchez, N., Seoane-Collazo, P., Jacas, J., Morgan, D.A., Serra, D., Gallego, R., Gonzalez, F., Casals, N., et al. (2014). Central ceramide-induced hypothalamic lipotoxicity and ER stress regulate energy balance. Cell Rep. *9*, 366–377. https://doi.org/10.1016/J.CELREP.2014.08.057.

61. Buxton, O.M., Cain, S.W., O'Connor, S.P., Porter, J.H., Duffy, J.F., Wang, W., Czeisler, C.A., and Shea, S.A. (2012). Adverse metabolic consequences in humans of prolonged sleep restriction combined with circadian disruption. Sci. Transl. Med. *4*, 129ra43. https://doi.org/10.1126/SCITRANSLMED.3003200.

62. Chaix, A., Zarrinpar, A., Miu, P., and Panda, S. (2014). Time-restricted feeding is a preventative and therapeutic intervention against diverse nutritional challenges. Cell Metabol. *20*, 991–1005. https://doi.org/10.1016/j.cmet.2014.11.001.

63. Anderson, S.T., and FitzGerald, G.A. (2020). Sexual dimorphism in body clocks. Science *369*, 1164–1165. https://doi.org/10.1126/science.abd4964.

64. Mieda, M., and Sakurai, T. (2011). Bmal1 in the nervous system is essential for normal adaptation of circadian locomotor activity and food intake to periodic feeding. J. Neurosci. *31*, 15391–15396. https://doi.org/10.1523/jneurosci.2801-11.2011.

65. Husse, J., Leliavski, A., Tsang, A.H., Oster, H., and Eichele, G. (2014). The light-dark cycle controls peripheral rhythmicity in mice with a genetically ablated suprachiasmatic nucleus clock. Faseb. J. *28*, 4950–4960. https://doi.org/10.1096/FJ.14-256594.

66. Ralph, M.R., Foster, R.G., Davis, F.C., Menaker, M., and Menaker, M. (1990). Transplanted suprachiasmatic nucleus determines circadian period. Science *247*, 975–978. https://doi.org/10.1126/science.2305266.

67. Meijer, J.H., and Rietveld, W.J. (1989). Neurophysiology of the suprachiasmatic circadian pacemaker in rodents. Physiol. Rev. *69*, 671–707. https://doi.org/10.1152/physrev.1989.69.3.671.

68. Van den Pol, A.N., and Powley, T. (1979). A fine-grained anatomical analysis of the role of the rat suprachiasmatic nucleus in circadian rhythms of feeding and drinking. Brain Res. *160*, 307–326. https://doi.org/10.1016/0006-8993(79)90427-x.

69. Silver, R., Lehman, M.N., Gibson, M., Gladstone, W.R., and Bittman, E.L. (1990). Dispersed cell suspensions of fetal SCN restore circadian rhythmicity in SCN-lesioned adult hamsters. Brain Res. *525*, 45–58. https://doi.org/10.1016/0006-8993(90)91319-c.

70. Silver, R., LeSauter, J., Tresco, P.A., and Lehman, M.N. (1996). A diffusible coupling signal from the transplanted suprachiasmatic nucleus controlling circadian locomotor rhythms. Nature *382*, 810–813. https://doi.org/10.1038/382810a0.

71. Harrington, M.E., Rahmani, T., and Lee, C.A. (1993). Effects of damage to SCN neurons and efferent pathways on circadian activity rhythms of hamsters. Brain Res. Bull. *30*, 655–669. https://doi.org/10.1016/0361-9230(93)90097-U.

72. Morrison, S.F., Madden, C.J., and Tupone, D. (2014). Central neural regulation of brown adipose tissue thermogenesis and energy expenditure. Cell Metabol. *19*, 741–756. https://doi.org/10.1016/j.cmet.2014.02.007.

73. Yu, X.X., Lewin, D.A., Forrest, W., and Adams, S.H. (2002). Cold elicits the simultaneous induction of fatty acid synthesis and β-oxidation in murine brown adipose tissue: prediction from differential gene expression and confirmation in vivo. Faseb. J. *16*, 155–168. https://doi.org/10.1096/FJ.01-0568COM.

74. Enerbäck, S. (2010). Human Brown Adipose Tissue. Cell Metabol. *11*, 248–252. https://doi.org/10.1016/j.cmet.2010.03.008.

75. Barca-Mayo, O., and López, M. (2023). Estradiol and leptin: no engagement without CITED1. Trends Endocrinol. Metabol. *34*, 389–391. https://doi.org/10.1016/J.TEM.2023.04.002.

76. González-García, I., García-Clavé, E., Cebrian-Serrano, A., Le Thuc, O., Contreras, R.E., Xu, Y., Gruber, T., Schriever, S.C., Legutko, B., Lintelmann, J., et al. (2023). Estradiol regulates leptin sensitivity to control feeding via hypothalamic Cited1. Cell Metabol. *35*, 438–455.e7. https://doi.org/10.1016/J.CMET.2023.02.004.

77. Cai, W., Rambaud, J., Teboul, M., Masse, I., Benoit, G., Gustafsson, J.-Å., Delaunay, F., Laudet, V., and Pongratz, I. (2008). Expression Levels of Estrogen Receptor β Are Modulated by Components of the Molecular Clock. Mol. Cell Biol. *28*, 784–793. https://doi.org/10.1128/MCB.00233-07.

78. Abo, S.M.C., and Layton, A.T. (2021). Modeling the circadian regulation of the immune system: Sexually dimorphic effects of shift work. PLoS Comput. Biol. *17*, e1008514. https://doi.org/10.1371/JOURNAL.PCBI.1008514.

79. Cespedes Feliciano, E.M., Rifas-Shiman, S.L., Quante, M., Redline, S., Oken, E., and Taveras, E.M. (2019). Chronotype, Social Jet Lag, and Cardiometabolic Risk Factors in Early Adolescence. JAMA Pediatr. *173*, 1049–1057. https://doi.org/10.1001/JAMAPEDIATRICS.2019.3089.

80. Santhi, N., Lazar, A.S., McCabe, P.J., Lo, J.C., Groeger, J.A., and Dijk, D.J. (2016). Sex differences in the circadian regulation of sleep and waking cognition in humans. Proc. Natl. Acad. Sci. USA *113*, E2730–E2739. https://doi.org/10.1073/pnas.1521637113.

81. López, M., Varela, L., Vázquez, M.J., Rodríguez-Cuenca, S., González, C.R., Velagapudi, V.R., Morgan, D.A., Schoenmakers, E., Agassandian, K., Lage, R., et al. (2010). Hypothalamic AMPK and fatty acid metabolism mediate thyroid regulation of energy balance. Nat. Med. *16*, 1001–1008. https://doi.org/10.1038/nm.2207.

82. Contreras, C., and López, M. (2014). Ceramide sensing in the hippocampus: the lipostatic theory and Ockham's razor. Mol. Metabol. *3*, 90–91. https://doi.org/10.1016/j.molmet.2013.12.004.

83. Milbank, E., Dragano, N.R.V., González-García, I., Garcia, M.R., Rivas-Limeres, V., Perdomo, L., Hilairet, G., Ruiz-Pino, F., Mallegol, P., Morgan, D.A., et al. (2021). Small extracellular vesicle-mediated targeting of hypothalamic AMPKα1 corrects obesity through BAT activation. Nat. Metab. *3*, 1415–1431. https://doi.org/10.1038/s42255-021-00467-8.

84. Urisarri, A., González-García, I., Estévez-Salguero, Á., Pata, M.P., Milbank, E., López, N., Mandiá, N., Grijota-Martinez, C., Salgado, C.A., Nogueiras, R., et al. (2021). BMP8 and activated brown adipose tissue in human newborns. Nat. Commun. *12*, 5274. https://doi.org/10.1038/s41467-021-25456-z.

85. Seoane-Collazo, P., Rial-Pensado, E., Estévez-Salguero, A., Milbank, E., García-Caballero, L., Ríos, M., Liñares-Pose, L., Scotece, M., Gallego, R., Fern Andez-Real, J.M., et al. (2021). Activation of Hypothalamic AMP-Activated Protein Kinase Ameliorates Metabolic Complications of Experimental Arthritis, *74*, pp. 212–222. https://doi.org/10.1002/art.41950.

86. Rial-Pensado, E., Rivas-Limeres, V., Grijota-Martínez, C., Rodríguez-Díaz, A., Capelli, V., Barca-Mayo, O., Nogueiras, R., Mittag, J., Diéguez, C., and López, M. (2022). Temperature modulates systemic and central actions of thyroid hormones on BAT thermogenesis. Front. Physiol. *13*, 1017381. https://doi.org/10.3389/FPHYS.2022.1017381.

87. Milbank, E., Martinez, M.C., and Andriantsitohaina, R. (2016). Extracellular vesicles: pharmacological modulators of the peripheral and central signals governing obesity. Pharmacol. Ther. *157*, 65–83. https://doi.org/10.1016/j.pharmthera.2015.11.002.

88. González-García, I., Contreras, C., Estévez-Salguero, Á., Ruíz-Pino, F., Colsh, B., Pensado, I., Liñares-Pose, L., Rial-Pensado, E., Martínez de Morentin, P.B., Fernø, J., et al. (2018). Estradiol regulates energy balance by ameliorating hypothalamic ceramide-induce ER stress. Cell Rep. *25*, 413–423.e5. https://doi.org/10.1016/j.celrep.2018.09.038.

89. Martínez de Morentin, P.B., Lage, R., González-García, I., Ruíz-Pino, F., Martins, L., Fernández-Mallo, D., Gallego, R., Fernø, J., Señarís, R., Saha, A.K., et al. (2015). Pregnancy induces resistance to the anorectic effect of hypothalamic malonyl-CoA and the thermogenic effect of hypothalamic AMPK inhibition in female rats. Endocrinology *156*, 947–960. https://doi.org/10.1210/EN.2014-1611.

90. Gonzalez-Rellan, M.J., Fondevila, M.F., Fernandez, U., Rodríguez, A., Varela-Rey, M., Veyrat-Durebex, C., Seoane, S., Bernardo, G., Lopitz-Otsoa, F., Fernández-Ramos, D., et al. (2021). O-GlcNAcylated p53 in the liver modulates hepatic glucose production. Nat. Commun. *12*, 5068. https://doi.org/10.1038/s41467-021-25390-0.

91. Seoane-Collazo, P., Roa, J., Rial-Pensado, E., Liñares-Pose, L., Beiroa, D., Ruíz-Pino, F., López-González, T., Morgan, D.A., Pardavila, J.Á., Sánchez-Tapia, M.J., et al. (2018). SF1-specific AMPKalpha1 deletion protects against diet-induced obesity. Diabetes *67*, 2213–2226. https://doi.org/10.2337/db17-1538.

92. Imbernon, M., Sanchez-Rebordelo, E., Romero-Picó, A., Kalló, I., Chee, M.J., Porteiro, B., Al-Massadi, O., Contreras, C., Fernø, J., Senra, A., et al. (2016). Hypothalamic kappa opioid receptor mediates both diet-induced and melanin concentrating hormone–induced liver damage through inflammation and endoplasmic reticulum stress. Hepatology *64*, 1086–1104. https://doi.org/10.1002/HEP.28716.

93. López, M., Lage, R., Saha, A.K., Pérez-Tilve, D., Vázquez, M.J., Varela, L., Sangiao-Alvarellos, S., Tovar, S., Raghay, K., Rodríguez-Cuenca, S., et al. (2008). Hypothalamic Fatty Acid Metabolism Mediates the Orexigenic Action of Ghrelin. Cell Metabol. *7*, 389–399. https://doi.org/10.1016/j.cmet.2008.03.006.

94. Heras, V., Castellano, J.M., Fernandois, D., Velasco, I., Rodríguez-Vazquez, E., Roa, J., Vazquez, M.J., Ruiz-Pino, F., Rubio, M., Pineda, R., et al. (2020). Central ceramide signaling mediates obesity-induced precocious puberty. Cell Metabol. *32*, 951–966.e8. https://doi.org/10.1016/j.cmet.2020.10.001.

95. Barca, O., Devesa-Peleteiro, P., Seoane, M., Señarís, R.M.A., and Arce, V.M. (2010). Bimodal effect of interferon-β on astrocyte proliferation and survival: Importance of nuclear factor-κB. J. Neuroimmunol. *226*, 73–80. https://doi.org/10.1016/J.JNEUROIM.2010.05.036.

96. Barca, O., Carneiro, C., Costoya, J.A., Señarís, R.M., and Arce, V.M. (2010). Resistance of neonatal primary astrocytes against Fas-induced apoptosis depends on silencing of caspase 8. Neurosci. Lett. *479*, 206–210. https://doi.org/10.1016/J.NEULET.2010.05.057.

97. Barca, O., Seoane, M., Ferré, S., Prieto, J.M., Lema, M., Señarís, R., and Arce, V.M. (2007). Mechanisms of Interferon-β-Induced Survival in Fetal and Neonatal Primary Astrocytes. Neuroimmunomodulation *14*, 39–45. https://doi.org/10.1159/000107287.

98. Seoane-Collazo, P., Liñares-Pose, L., Rial-Pensado, E., Romero-Picó, A., Moreno-Navarrete, J.M., Martínez-Sánchez, N., Garrido-Gil, P., Iglesias-Rey, R., Morgan, D.A., Tomasini, N., et al. (2019). Central nicotine induces browning through hypothalamic κ opioid receptor. Nat. Commun. *10*, 4037. https://doi.org/10.1038/S41467-019-12004-Z.

STAR★METHODS

KEY RESOURCES TABLE

REAGENT or RESOURCE	SOURCE	IDENTIFIER
Antibodies		
Mouse anti-GFAP (1:1000)	Sigma-Aldrich	G3893, RRID: AB_477010
Rabbit anti-BMAL1 (1:1000, western blot; 1:200, immunofluorescence)	Santa Cruz Biotechnology	sc-365645, RRID: AB_10841724
Rabbit anti-UCP-1 (1:5000, western blot; 1:2000, immunohistochemistry)	Abcam	ab10983; RRID: AB_2241462
Rabbit anti-ACC (1:1000)	Cell Signaling	3662-S, RRID: AB_10694075
Mouse anti-FAS (1:1000)	BD Science	610963, RRID: AB_398276
Mouse anti-SREBP1c (1:1000)	Abcam	ab3259, RRID: AB_303650
Rabbit anti-phospho-HLS (1:1000)	Cell Signaling	4126, RRID: AB_490997
Rabbit anti-HSL (1:1000)	Abcam	ab45422, RRID: AB_2135367
Mouse anti-GAPDH (1:5000)	Santa Cruz Biotechnology	sc-25778, RRID: AB_10167668
Mouse anti-α-tubulin (1:5000)	Sigma-Aldrich	T5168; RRID: AB_477579
Mouse anti-β-Actin (1:5000)	Sigma-Aldrich	A5316; RRID: AB_476743
Alexa Fluor 488 Goat anti-Rabbit IgG (H + L) (1:1000)	Invitrogen	A11008; RRID: AB_143165
Alexa Fluor 546 Goat anti-Mouse IgG2b (1:1000)	Invitrogen	A21143; RRID: AB_2535779
Alexa Fluor® 647 Nano-Secondary alpaca anti-mouse IgG1 (1:1000)	Proteintech	sms1AF647-1; RRID: AB_2864264
Bacterial and virus strains		
AAV (serotype 2/5)- GFAP (2.2)-iCre	Vector Biolabs	VB1172
AAV (serotype 2/5)- GFAP (2.2)-EGFP	Vector Biolabs	VB1180
Chemicals, peptides, and recombinant proteins		
Tamoxifen	Sigma-Aldrich	Cat# T5648
D-glucose	Sigma-Aldrich	Cat# G8270
Insulin	Novo Nordisk	N/A
Protease inhibitor cocktail tablets	Roche Diagnostics	Cat# 11697498001
Ethylenediaminetetraacetic acid disodium salt dihydrate	Sigma-Aldrich	Cat# E5134
Ethylene glycol-bis(β-aminoethyl)-N, N, N', N'-tetra acetic Acid	Merck	Cat# 324626
Sodium Orthovanadate	Sigma-Aldrich	Cat# S6508
Sodium Fluoride	Sigma-Aldrich	Cat# 201154
Sodium chloride	Sigma-Aldrich	Cat# 1-06404
Sodium pyrophosphate	Sigma-Aldrich	Cat# 221368
Sucrose	Sigma-Aldrich	Cat# S0389
Corn Oil	Sigma-Aldrich	Cat# C8267
Tween 20	Sigma-Aldrich	Cat# P9416
Paraformaldehyde	Sigma-Aldrich	Cat# P6148
Bovine serum albumin	Sigma-Aldrich	Cat# A9647
Methanol	Sigma-Aldrich	Cat# 179337
Chloroform	Sigma-Aldrich	Cat# 32211
Tritón X-100	Sigma-Aldrich	Cat# 282103
Protein Assay Dye Reagent	BIO RAD	Cat# #5000006

(*Continued on next page*)

Continued		
REAGENT or RESOURCE	SOURCE	IDENTIFIER
β3-AR specific antagonist, SR59230A	TOCRIS	Cat# 1511/10
Critical commercial assays		
Mouse Leptin ELISA	Merck-Millipore	Cat# EZML-82K
Mouse Insulin ELISA	Merck-Millipore	Cat# EZRMI-13K
Triglycerides colorimetric assay	Spinreact	Cat# 1001314
Cholesterol colorimetric assay	Spinreact	Cat# 1001093
ImProm-II™ Reverse Transcription System	Promega	Cat# A3800
QuantiFast SYBR Green PCR Kit	Qiagen	Cat# 204054
Experimental models: Organisms/strains		
Bmal1$^{flx/flx}$ (B6.129S4(Cg) Arntltm1Weit/J)	Jackson Laboratory	RRID: IMSR_JAX:007668
Glast-CreER^{T2}	Magdalena Götz, Ludwig-Maximilians-University Munich	(Mori et al.)[27]
td-Tomato (B6. Cg-Gt (ROSA)26Sor tm9 (CAG-tdTomato)Hze/J)	Jackson Laboratory	RRID: IMSR_JAX:007909
Oligonucleotides		
See Table S1 list of primers used in this paper		N/A
Software and algorithms		
GraphPad Prism v9.5.1	GraphPad Software	https://www.graphpad.com/
ImageJ v1.53c	NIH	https://imagej.nih.gov/ij/download.html
FLIR Tools software	FLIR Systems	N/A
ANY-maze software	Stoelting	N/A
TSE Systems	LabMaster	N/A
Minispec	BRUKER	N/A
Wheel Manager software	SOF-860- Med Associates Inc	N/A
Actogram J	ImageJ	https://bene51.github.io/ActogramJ/
Other		
Standard chow diet (Teklad Global 18% Protein Roden Diet)	ENVIGO Company	Cat# 2918
HFD (60% fat, 20% carbohydrate, 20% protein, 5.21 kcal/g; D12492)	Research Diets	Cat# D12492

RESOURCE AVAILABILITY

Lead contact

Further information and requests for resources and reagents should be directed to and will be fulfilled by the lead contact, Olga Barca-Mayo (olga.barca.mayo@usc.es).

Materials availability

This study did not generate new unique reagents.

Data and code availability

All data reported in this paper will be shared by the lead contact upon request. This paper does not report original code. Any additional information required to reanalyze the data reported in this paper is available from the lead contact upon request.

EXPERIMENTAL MODEL AND STUDY PARTICIPANT DETAILS

Animals

Mice were housed with *ad libitum* access to food and water and kept on a 12-h (8 a.m.–8 p.m.) light-dark cycle in a room maintained at 21°C at the animal facility of the University of Santiago de Compostela. Care of all animals followed institutional animal care

committee guidelines. All procedures were reviewed and approved by the University of Santiago de Compostela Ethics Committee, following the European Union normative for the use of experimental animals (Project ID 15012/2021/011).

Bmal1$^{flx/flx}$ (B6.129S4(Cg) Arntltm1Weit/J; RRID: IMSR_JAX:007668) and *td-Tomato* (B6. Cg-Gt(ROSA)26Sor tm9 (CAG-tdTomato)Hze/J; RRID:IMSR_JAX:007909) mice were obtained from Jackson Laboratory, and the *Glast*-CreER^{T2} mouse line was kindly provided by from Dr. M. Götz (Ludwig-Maximilians-University Munich, Germany).

METHOD DETAILS

Treatments

Eight-to ten-week-old Glast-CreER^{T2}; *Bmal1*$^{flx/flx}$ (*Bmal1cKD*) mice and controls (*Bmal1*$^{flx/flx}$) were treated with Tamoxifen (Sigma-Aldrich, T-5648) dissolved in corn oil (Sigma-Aldrich, C-8267).[11,17,26] The animals received 5 mg/day for two days by oral gavage,[11,17,26,27] and *Bmal1*$^{flx/flx}$ littermates treated with tamoxifen served as controls. Animals were provided *ad libitum* access to water and either standard chow (ENVIGO Company) or a high-fat diet (60% fat, 20% carbohydrate, 20% protein, 5.21 kcal/g; D12492; Research Diets, Inc) starting one week after the TM treatment. Body weights and food intake were measured weekly.

The β3-AR specific antagonist, SR59230A ([3-(2ethylphenoxy)-1-[(1,S)-1,2,3,4-tetrahydronapth-1-ylamino]-2S-2-propanol-oxalate] (3 mg/kg/day, dissolved in DMSO; Tocris Bioscience; Bristol, UK)[57,58,81,82] was administrated subcutaneously for 7 days twice a day, at the onset of the cycles at 8:00 and 20:00.

Determination of the body composition

The whole-body composition was measured using nuclear magnetic resonance imaging (Whole Body Composition Analyzer; EchoMRI, Houston, TX).

Thermographic temperature

Skin temperature surrounding BAT was recorded using a B335 compact infrared thermal imaging camera (FLIR) and analyzed with FLIR Tools software (FLIR Systems).[83–86] Infrared thermography images were taken from the back of the mice to precisely visualize heat production from the BAT. For each image, the BAT surrounding area was delimited, and the average temperature of the skin area was calculated as the average of 3 pictures per mouse.

Indirect calorimetry

Mice were analyzed for energy expenditure, respiratory quotient, and spontaneous locomotor activity using a calorimetric system (LabMaster; TSE Systems).[58,83,85,87] Mice were acclimated for 24 h to the test chambers and then monitored for an additional 48–96 h.

Ovariectomy

Four weeks after TM treatment, female mice in the control and *Bmal1cKD* groups underwent bilateral ovariectomy (OVX) or sham surgery.[58,88,89] Briefly, under ketamine–xylazine anesthesia (50 mg/kg, intraperitoneal), both flanks of the mice were shaved, and they were placed on their left flank. An incision was made in the right flank skin and muscle layers, and the ovary was carefully extracted. The distal part of the uterine horn was ligated with a surgical suture, and then the ovary was removed by dissecting between the suture and the ovary. The same procedure was performed to remove the left ovary after returning the horn to the abdominal cavity. The wound was closed by suturing the muscle layer with surgical silk and applying surgical staples to the skin. Sham surgeries were also performed, where each ovary was exposed but not tied or dissected. All experimental tests on OVX mice were conducted four weeks after surgery to ensure complete washout of ovarian hormones.[58,88,89]

Stereotaxic microinjections of AAV

To specifically ablate BMAL1 in mediobasal (MBH) or arcuate (ARC) astrocytes, we utilized adeno-associated virus (AAV) viral particles (serotype 2/5) that expressed GFP or Cre protein under the control of the hGFAP promoter (Vector Biolabs, Philadelphia, PA, USA). AAV-hGFAP-GFP (control animals) or AAV-hGFAP-Cre (GFAP-Bmal1-KD) particles (2×10^9 viral genome particles per side) were stereotaxically injected bilaterally into the MBH or ARC of *Bmal1*$^{fl/fl}$ littermates. The injections were performed using a 33-gauge needle connected to a 1 mL syringe (Neuro-Syringe, Hamilton). Stereotaxic coordinates were −1.5 mm posterior, −0.4 mm lateral to bregma; and −5.8 mm ventral from the dura for the MBH and −2.8 mm posterior, ±0.3 mm lateral to bregma and 10.2 mm dorsoventral for the ARC.[57–60] Before retracting the needle, a 10-min time-lapse was allowed to prevent backflow through the needle track, and then the syringe was withdrawn. After the procedure, the skin incision was closed with surgical sutures (Henry Schein), and mice were placed in a heated cage until they recovered from anesthesia. Body weight and food intake were monitored weekly. Experiments were conducted at least three weeks after the injections to ensure AAV expression. Surgeries were performed using a mixture of ketamine and xylazine (15 mg/kg and 3 mg/kg) as anesthetic agents, and meloxicam (5 mg/kg) and buprenorphine (0.05 mg/kg) were administered as analgesic agents.

Open field test

Two months after TM treatment, control andBmal1cKD mice were habituated to handling and transport from the colony room to the behavioral room for 3 days before the tests began. The tests were conducted during the light cycle (ZT 3–7). Each mouse was placed in a brightly lit 44 × 44 cm acrylic square box, and their activity was tracked using an overhead FireWire camera (DMK 31AF03-Z2, The Imaging Source). The animal's activity was recorded every 5 min for 1 h on day 1, and the same procedure was repeated 24 h later, on day 2. The recorded data were analyzed using ANY-maze software (Stoelting). Throughout the experiments, the investigators were blinded to group allocation. All apparatuses and testing chambers were cleaned with 70% ethanol wipes between each animal.

Circadian locomotor activity

Female *Bmal1cKD* and control mice, aged 4–5 months, were single-housed in cages equipped with running wheels (ENV-044; Med Associates Inc). The mice were given a 3-day adaptation period to the wheels in standard light-dark cycles (12 h:12 h) before the start of the experiment. The experiment was conducted under these light-dark cycle conditions for 7–10 days. Subsequently, the mice were transferred to isolated black cages (Tecniplast) and placed in constant darkness for 30 days. After the constant darkness period, the mice were exposed to light-dark cycles (12 h:12 h) for ten days. Running wheel activity was recorded in 5-min bins using Wheel Manager software (SOF-860; Med Associates Inc). The data obtained were analyzed with Actogram J (https://bene51.github.io/ActogramJ/).[11,17]

Food restriction experiments

Control and *Bmal1cKD* mice, after 12 weeks of TM treatment, were housed in a temperature- and humidity-controlled room under a 12:12 h light-dark cycle (LD) with lights on at 08:00 (ZT0). To minimize potential effects of different body weights between genotypes on the acquisition of the food anticipatory activity (FAA), mice were subjected to the restricted feeding (RF) paradigm 12 weeks after TM when the differences between sex-matched groups were reduced. Prior to the restricted feeding schedules, locomotor activity was monitored in LD for seven days under *ad libitum* (AL) feeding conditions. Body weight and food intake were determined at ZT4. Subsequently, the mice were exposed to a restricted feeding schedule for ten days. During this schedule, access to standard lab chow (ENVIGO Company) was restricted from ZT4 to ZT10 for six days and from ZT4 to ZT8 for the remaining four days. To monitor food consumption, food pellets for each mouse were weighed daily before (ZT4) and after (ZT10 or ZT8) food availability.

Running wheel activity was recorded in 5-min bins using Wheel Manager software (SOF-860; Med Associates Inc). The activity data were analyzed by Actogram-J, and actograms and average waveforms were generated for visual inspection. The acrophases were obtained by fitting the average activities to a cosinor curve with a period of 24 h. The equation used for the nonlinear least-squares regression fitting was $y = A + B \times \cos[2\pi \times (t-C)/24]$, where A is the rhythm-adjusted mean, B is the amplitude of the rhythm, C is the phase given in circadian time, and t is the circadian time. Food anticipatory activity (FAA) was defined as occurring 4 h preceding the scheduled mealtime. FAA was calculated by dividing the locomotor activity in the 4 h before the scheduled feeding by the total amount of locomotor activity over 24 h, expressed as a percentage of the total. Similarly, nocturnal activity was calculated by dividing the locomotor activity at night (ZT12 - ZT24) by the total locomotor activity over 24 h, including the FAA.

Glucose and insulin tolerance test

Insulin tolerance tests (ITT) were performed in 6 h food-deprived mice. For the glucose tolerance test (GTT) an intraperitoneal injection of 2 g/kg of D-glucose (G8270, Sigma-Aldrich) was administered, while for the ITT, an injection of insulin (0.75 IU/kg for males and 0.35 IU/kg for females) (Actrapid, Novo Nordisk) was given.[17,90,91] Blood glucose levels were measured at the indicated time points.

Glucose-stimulated insulin secretion

An intraperitoneal injection of 2 g/kg of D-glucose (G8270, Sigma-Aldrich) was administered. Blood samples were collected at different time points and insulin levels were measured using an Insulin Mouse enzyme-linked immunosorbent assay (ELISA) kit (Millipore, USA).[17]

Determination of metabolic markers

To determine circulating levels of cholesterol and triglycerides, spectrophotometry was performed using a Multiskan GO spectrophotometer(Invitrogen-ThermoFisher) with specific kits (cholesterol kit no. 1001093 and triglycerides kit no. 1001314, Spinreact).

For quantification of liver triglycerides, liver tissues were homogenized in ice-cold chloroform-methanol (2:1 v/v).[57,92] Liver triglycerides were extracted by shaking the samples for 3 h at room temperature. Phase separation was achieved by adding miliQ water, followed by centrifugation, and collection of the organic bottom layer. The organic solvent was then dried at room temperature overnight using a Speed Vac and the residue was dissolved in chloroform. The triglyceride content of each sample was measured in duplicate using a colorimetric assay (Spinreact, Girona, Spain) after evaporation of the organic solvent.

Immunofluorescence

To confirm Cre-mediated recombination, we crossed Glast-CreER^{T2} mice with a reporter mouse line that expresses a red fluorescent reporter protein, Td-TOMATO, under the control of the CAG promoter upon Cre-mediated recombination of *loxP* sites.[11,17,26]

Immunofluorescence analysis was performed two months after TM treatment to examine Glast-Cre-mediated recombination and the immunoreactivity of the astrocyte-specific marker, glial fibrillary acidic protein (GFAP), in the suprachiasmatic and arcuate nucleus.[11,17,26]

Mice were anesthetized with ketamine/xylazine (150 mg/kg, 10 mg/kg) and perfused transcardially with ice-cold PBS followed by ice-cold 4% PFA.[11,17,26] The brains were post-fixed overnight in 4% PFA in PBS, and 30 μm thick slices were prepared using a cryostat (Leica). The slices were permeabilized with 0.3% Triton X-100 in PBS, blocked with 10% goat serum in PBS, and incubated overnight at 4°C with primary antibodies: mouse anti-GFAP (dilution 1:1000, Sigma, G3893) and rabbit anti-Bmal1 (dilution 1:200, Santa Cruz Biotechnology, sc-365645). The following day, the sections were extensively washed and incubated for 2 h with goat anti-rabbit or anti-mouse Alexa 488 or Alexa 546 secondary antibodies (dilution 1:1000). After additional washing steps, the slices were mounted with Prolong Gold and imaged using an inverted laser scanning confocal microscope (Leica TCS SP5) with a 20x or 40× objective (Leica Microsystems). Quantification and analysis were performed using ImageJ software (Wayne Rasband, NIH, USA) by outlining the hypothalamus from the Dapi-stained image and measuring the relative intensity of the immunostaining. When multiple sections were analyzed from each animal, the mean of the measurements from consecutive sections was used for that individual.

RNA isolation and quantitative RT-PCR

Livers samples were collected for RNA isolation at the specific time points of interest from animals maintained under a 12-h light-dark cycle. Total RNA was extracted using TRIzol reagent (Invitrogen), according to the manufacturer's instructions. Subsequently, cDNA was synthesized by reverse transcribing 0.5 μg of total mRNA using the ImProm-II Reverse Transcription System (Promega) following the manufacturer's instructions. Quantitative real-time RT-PCR was performed using the ABI PRISM.7900 (Applied Biosystems). For a 15 μL reaction, 9 ng of cDNA template was mixed with primers to a final concentration of 200 nM, and 7.5 μL of 2x QuantiFast SYBR Green PCR Master Mix (Qiagen) was added. The reactions were run in duplicate under the following conditions 5 min at 95°C, followed by 40 cycles of 10 s at 95°C, 30 s at 60°C, and 1 min at 70°C. Gapdh transcripts were used as reference controls for normalization purposes.

Western blotting

Tissues including brown and gonadal adipose tissue, livers, and hypothalamus were homogenized in lysis buffer containing 0.05 M Tris-HCl, 0.01 M EGTA, 0.001 M EDTA, 0.016 M Triton X-100, 0.001 M sodium orthovanadate, 0.05 M sodium fluoride, 0.01 M sodium pyrophosphate, and 0.25 M sucrose. The lysis buffer was prepared with distilled water and adjusted to a pH of 7.5 using reagents from Sigma-Aldrich. Freshly added protease inhibitor cocktail tablets from Roche Diagnostics (Indianapolis, IN, USA) were included. The protein concentration was determined by the Bradford Method (Protein assay dye concentrate, Bio-Rad Laboratories), and the total protein content of the tissues was calculated. The protein lysates were separated by 10% SDS-PAGE and transferred onto nitrocellulose membranes (Protran, Schleicher and Schuell, Dassel, Germany).[11,17,86] The membranes were probed with specific antibodies against the following proteins: BMAL1 (Abcam, ab93806) at a dilution of 1:1000; (Abcam, ab93806) at a dilution of 1:1000, ACC (Cell Signaling, 3662-S) at a dilution of 1:1000, UCP1 (Abcam, AB_631364) at a dilution of 1:10000, FAS (BD Science, 610963) at a dilution of 1:1000, SREBP1c (Abcam, AB3259) at a dilution of 1:1000, phospho-HLS (Ser660) (AB_490997, Cell Signaling Technology), and HSL (Abcam, ab45422).[11,58,93,94] Subsequently, the membranes were washed and re-probed with antibodies against GAPDH (Santa Cruz, FL-335: sc-25778) at a dilution of 1:5000, β-ACTIN (Sigma-Aldrich, A5316), or α-TUBULIN (Sigma-Aldrich, AB_330337) at a dilution of 1:5000 as the loading control. Immunoreactive bands were detected using a chemiluminescence detection system (ECL, GE Healthcare Bio-Sciences AB). Autoradiographic films (Fujifilm, Tokyo, Japan) were scanned, and the band signal was quantified by densitometry using ImageJ 1.33 software (NIH).[11,58,83,85,93–97] The values were expressed relative to GAPDH, α-TUBULIN, or β-ACTIN. Representative images for all proteins are shown. For the loading controls, a representative gel is displayed, although each protein was normalized to its respective internal control (GAPDH, α-TUBULIN, or β-ACTIN). In all the figures showing gel images, all the bands for each picture are from the same gel, although they may be spliced for clarity.

Histological analysis

BAT and liver samples were fixed in 10% formalin buffer for 24 h and then dehydrated and embedded in paraffin by a standard procedure. Sections of 3 μm were prepared with a microtome and stained using a standard Hematoxylin/Eosin Alcoholic (BioOptica) procedure according to the manufacturer's instruction. BAT sections were used for immunohistochemistry detection of UCP-1, using a rabbit anti-UCP-1 (1:2000; Abcam). UCP-1-positive cells were quantified with ImageJ analysis software.[83,85,91,98] Hepatic lipid content was analyzed by Oil Red O staining.[88] Lipids in Oil Red O-stained sections were quantified using ImageJ software. 4 to 6 animals per experimental group were used, and three pictures per section were analyzed. All analyzed values are represented with respect to control (100%).

QUANTIFICATION AND STATISTICAL ANALYSIS

Data are presented as mean ± SEM and were analyzed and graphed using Prism 6 (GraphPad, San Jose, CA, USA). Statistical parameters, including the exact value of n and precision measures (mean ± s.e.m.) and statistical significance, are reported in the Figures and Figure Legends. All statistical tests were two-sided. Unpaired Student's t-test was used to compare two groups from

different genotypes. To compare the differences between ZT or days and genotype, data were analyzed by two-way ANOVA followed by Bonferroni's post-hoc test for multiple comparisons. Data were checked for normality and equal variances between groups. Indirect calorimetry data were analyzed using two-way ANOVA for repeated-measures with a Bonferroni's post hoc test if required. Mean values corresponding to the entire light or dark phases separately are represented by histograms and were analyzed by unpaired Student's t-test. The data from indirect calorimetry were analyzed by ANCOVA followed by Bonferroni's posthoc test, using the metabolic parameter (energy expenditure, VO_2 consumption, VCO_2 production, feeding) as a dependent variable, genotype as a factor and body weight as a covariate. The statistical significance of the rhythmic expression of the locomotor activity, metabolic cycles or gene expression was determined by Cosinor analysis.[9,11,17,26] The periods and acrophases were obtained from the cosinor curve.

The cutoff for significance was * = $p < 0.05$, ** = $p < 0.01$, *** = $p < 0.001$ and **** = $p < 0.0001$.

Samples or animals were excluded from the data analysis with pre-established criteria if they deviated more than two SD from the group mean.